Available online at www.sciencedirect.com

SciVerse ScienceDirect

Geochimica et Cosmochimica Acta 99 (2012) 39–56

Geochimica et Cosmochimica Acta

www.elsevier.com/locate/gca

Reconstruction of the Nd isotope composition of seawater on epicontinental seas: Testing the potential of Fe–Mn oxyhydroxide coatings on foraminifera tests for deep-time investigations

Guillaume Charbonnier [a,b,*], Emmanuelle Pucéat [b], Germain Bayon [c], Delphine Desmares [d], Guillaume Dera [e], Christophe Durlet [b], Jean-François Deconinck [b], Francis Amédro [b], Alexandra T. Gourlan [f], Pierre Pellenard [b], Brahimsamba Bomou [g]

[a] *UMR CNRS 8148 Interactions et Dynamique des Environnements de Surface, Université Paris Sud XI, Bâtiment 504, 91405 Orsay, France*
[b] *UMR CNRS 6282 Biogéosciences, 6 Bd. Gabriel, 21000 Dijon, France*
[c] *IFREMER, Unité de Recherche Géosciences Marines, F-29280 Plouzané, France*
[d] *UPMC Univ Paris 06, UMR 7207, CR2P, 4 Place Jussieu, 75252 Paris, France*
[e] *UMR CNRS 5563 Géosciences Environnement Toulouse, 14 Avenue Edouard Belin, 31400 Toulouse, France*
[f] *UMR CNRS 5025 Géodynamique des Chaines Alpines (GCA), 1381 rue de la piscine, 38041 Grenoble, France*
[g] *Institut de Géologie et Paléontologie, Quartier UNIL-Dorigny Bâtiment Anthropole, CH-1015 Lausanne, Switzerland*

Received 6 October 2011; accepted in revised form 5 September 2012; available online 24 September 2012

Abstract

The Fe–Mn oxide fraction leached from deep-sea sediments has been increasingly used to reconstruct the Nd isotope composition of deep water masses, that can be used to track changes in oceanic circulation with a high temporal resolution. Application of this archive to reconstruct the Nd isotope composition of bottom seawater in shallow shelf environments remained however to be tested. Yet as the Nd isotope composition of seawater on continental margins is particularly sensitive to changes in erosional inputs, establishment of neritic seawater Nd isotope evolution around areas of deep water formation would be useful to discriminate the influence of changes in oceanic circulation and in isotopic composition of erosional inputs on the Nd isotope record of deep waters. The purpose of this study is to test the potential of Fe–Mn coatings leached from foraminifera tests to reconstruct the Nd isotope composition of seawater in shelf environments for deep-time intervals. Albian to Turonian samples from two different outcrops have been recovered, from the Paris Basin (Wissant section, northern France) and from the Western Interior Seaway (Hot Spring, South Dakota, USA), that were deposited in epicontinental seas. Rare Earth Element (REE) spectra enriched in middle REEs in the foraminifera leach at Wissant highlight the presence of Fe–Mn oxides. The similarity of the Nd isotopic signal of the Fe–Mn oxide fraction leached from foraminifera tests with that of fish teeth suggests that Fe–Mn oxides coating foraminifera can be good archives of shelf bottom seawater Nd isotopic composition. Inferred bottom shelf water Nd isotope compositions at Wissant range from −8.5 to −9.7 ε-units, about 1.5–2 ε-units higher than that of the contemporaneous local detrital fraction. At Hot Spring, linear REE spectra characterizing foraminifera leach may point to an absence of authigenic marine Fe–Mn oxide formation in this area during the Late

* Corresponding author at: UMR CNRS 8148 Interactions et Dynamique des Environnements de Surface, Université Paris Sud XI, Bâtiment 504, 91405 Orsay, France.
E-mail address: guillaume.charbonnier@u-psud.fr (G. Charbonnier).

http://dx.doi.org/10.1016/j.gca.2012.09.012

Cenomanian–Early Turonian, consistent with dysoxic to anoxic conditions at Hot Spring, contemporaneous to an Oceanic Anoxic Event. The similarity of the Nd isotopic signal of the carbonate matrix of foraminifera with that of fish teeth suggests that it records the Nd isotope composition of bottom shelf seawater as well. Inferred bottom shelf water Nd isotope compositions at Hot Spring are quite radiogenic, between −7 and −6 ε-units, about 2.5–4 ε-units higher than that of the contemporaneous local detrital fraction. In contrast, in both sections Fe–Mn oxides leached directly from the decarbonated sediment tend to yield a less radiogenic Nd isotopic composition, typically between 0.2 and 0.8 ε-units lower, that is intermediate between that of fish teeth and of the detrital fraction. This suggests the contribution of pre-formed continental Fe–Mn oxides to the Nd isotopic signal, along with authigenic marine oxides, or a detrital contamination during leaching.

1. INTRODUCTION

The neodymium isotopic composition ($^{143}Nd/^{144}Nd$ ratio, expressed as ε_{Nd}) of seawater has been widely used to reconstruct past changes in oceanic circulation in both modern and ancient oceans (e.g. Thomas, 2004; Piotrowski et al., 2005; Robinson et al., 2010). Nd in seawater ultimately derives from continents, and the rocks eroded around the oceanic basins imprint each basin with a distinct isotopic composition depending on the age and lithology of the rock (Piepgras et al., 1979; Goldstein and O'Nions, 1981; Frank, 2002). The short residence time of Nd in the ocean (~300 to ~600 years; Frank, 2002; Tachikawa et al., 2003; Arsouze et al., 2009) compared to the oceanic mixing time (~1500 years; Broecker and Peng, 1982) prevents complete homogenization but is long enough for Nd to be transported by deep water masses along their pathways. At present, the unradiogenic signature of North Atlantic Deep Water ($\varepsilon_{Nd} = -13.5 \pm 0.5$) derives from the contribution of Nd from Archean and Proterozoic continental rocks in northern Canada and Greenland (Piepgras and Wasserburg, 1987; Lacan and Jeandel, 2005a,b). In contrast, the Pacific Ocean has a more radiogenic composition ($\varepsilon_{Nd} = 0$ to -5) that reflects the weathering of island arc material (Piepgras and Jacobsen, 1988; Shimizu et al., 1994; Amakawa et al., 2004, 2009).

Although it is established that the continents are the major source of Nd, the processes that deliver Nd to the ocean are still discussed (e.g. Arsouze et al., 2007, 2009; Siddall et al., 2008; Rempfer et al., 2011). An increasing number of recent studies emphasize the importance of processes occurring at the ocean margins, interaction between sediments and seawater (termed "boundary exchanges") and submarine groundwater discharge (Lacan and Jeandel, 2005a; Johannesson and Burdige, 2007; Jeandel et al., 2007; Arsouze et al., 2009), and of reversible scavenging (i.e. surface removal of Nd followed by remineralization at depth (Siddall et al., 2008). Importantly, boundary exchange along continental margins surrounding areas of deep water formation is involved in the acquisition of the Nd isotope composition of deep water masses, as has been shown for the North Atlantic Deep Waters (Lacan and Jeandel, 2004a,b,c, 2005a,b). Since the composition of seawater flowing along margins and on shelf can be significantly modified by boundary exchange-type processes (Lacan and Jeandel, 2005b; Carter et al., 2012), knowledge of the Nd isotope signature of shelf waters surrounding the regions of deep water formation and their evolution though time appear crucial for a robust interpretation of the evolution of ε_{Nd} depicted in deep waters. Indeed changes in oceanic circulation as well as changes in the ε_{Nd} of the material eroded in the region of deep water formation can modify the ε_{Nd} composition of a deep water mass (e.g. Vance and Burton, 1999; Thomas, 2004). Comparison of deep water Nd isotope evolution with that of seawater on the continental margins surrounding the source area could then help discriminate between these two processes.

Paleoceanographic studies based on ε_{Nd} are now commonly conducted on deep-time periods like the Eocene, Paleocene, or Cretaceous (e.g. Thomas, 2004; MacLeod et al., 2008; Gleason et al., 2009; Robinson et al., 2010; Martin et al., 2012). Yet several intervals within these deep-time periods, particularly the Cretaceous, are characterized by high sea-level, and large epicontinental seas covered part of the continents, that have no modern equivalent. During the transgression maximum of the Cenomanian–Turonian interval for instance, a large epicontinental sea, the Western Interior Seaway, extended 6000 km from south to north of North America, over up to 2000 km of width. For these periods of time, boundary exchanges may have been favored by the existence of epicontinental seas around the regions of potential deep water formation. The ε_{Nd} of the local bottom waters in these quite shallow environments may then have been particularly important to determine the end-member composition of the sinking water masses in nearby open ocean. In addition, for the Cretaceous period, it has been suggested that warm and saline waters formed in the low-latitude areas covered with shallow epicontinental seas could have sunk to intermediate depth and played a role in the thermohaline circulation (Friedrich et al., 2008; Hay, 2008; MacLeod et al., 2008).

Fish debris, that acquire their Nd isotope composition from bottom seawater at the sediment–water interface during early diagenesis, have been widely used to reconstruct the evolution of past bottom ocean waters (e.g. Martin and Scher, 2004; Thomas, 2004; Martin et al., 2010). Yet they are not always abundant in marine sediments. To improve temporal resolution of reconstructed ε_{Nd} records, the neodymium isotopic composition of authigenic Fe–Mn oxide coatings on bulk marine sediments has been increasingly used in the last decade to reconstruct past changes in oceanic circulation (Rutberg et al., 2000; Piotrowski et al., 2005, 2008; Négrel et al., 2006; Gutjahr et al., 2008; Martin et al., 2010). It has been shown that Fe–Mn oxides coatings on sediment particles, that form under oxidizing conditions

at the sediment–water interface or below, depending on the depth where oxic and anoxic pore waters interface, record the ε_{Nd} of seawater at the bottom of the water column (Palmer and Elderfield, 1985; Bayon et al., 2002; Piotrowski et al., 2004, 2005; Gutjahr et al., 2008; Martin et al., 2010). However, partial mobilization of Nd from in situ detrital material during leaching procedures can in some case (e.g. presence in sediment of easily weathered volcanic ash) contribute to bulk sediment leachate record (Roberts et al., 2010; Elmore et al., 2011). In addition, close to continental margins, remobilization of shelf and upper continental slope sediments and their subsequent downslope transport can occur. A first generation of Fe–Mn oxyhydroxide coatings incorporating the Nd isotope signature of shelf waters can then be exported downslope and contribute significantly to the Nd isotope signal of deep-sea core bulk sediment coatings (Gutjahr et al., 2008; Stumpf et al., 2010). In proximal settings, further complication arises from the likely occurrence of oxides pre-formed on the continent and brought by erosion (Bayon et al., 2004), that would then contribute to the Nd isotopic signal of the Fe–Mn component along with authigenic marine oxides.

In order to avoid these complications, Nd isotopic measurements on postdepositional Fe–Mn oxide coatings precipitated on both planktic and benthic foraminifera tests have been successfully used in recent studies to reconstruct bottom water ε_{Nd} (Klevenz et al., 2008; Roberts et al., 2010; Elmore et al., 2011). Yet this technique has been restricted to deep-sea sediments and recent periods so far. In this work we explore the possibility of using the Fe–Mn phase leached on foraminifera tests recovered from shelf environments to reconstruct the ε_{Nd} of seawater on continental margins for deep-time intervals. An additional problem may arise from the formation of recent Fe–Mn oxides formed after exhumation (telogenesis) of the sediments, in meteoric oxidizing waters, that may contribute to the Nd signal of the leachate as well. Yet if proved reliable for neritic settings as well, this technique would provide a convenient way to obtain the Nd isotopic signature of seawater in shallow environments with a higher temporal resolution than is currently done in such an environment using the Nd isotope composition of fish remains, not always abundant in sediments (Pucéat et al., 2005; Soudry et al., 2006).

Samples have been recovered from two sedimentary basins and from formations of different age, the Paris Basin (Wissant outcrop, northern France, Late Albian) and the Western Interior Basin (Hot Springs outcrop, South Dakota, USA, Cenomanian–Turonian stage boundary), presenting different facies within shelf environments (clayey with phosphatic beds and carbonate-marl alternation respectively). The concentration in rare earth elements (REEs) and the Nd isotope composition of four different phases of the samples (leachate of foraminifera coatings, leachate of decarbonated sediments, fish teeth, and detrital fraction) are determined, and used to test the potential of the ε_{Nd} of Fe–Mn oxyhydroxide foraminifera coatings for paleoceanographic reconstructions.

2. GEOLOGICAL CONTEXT

Samples were recovered from two sections (Wissant and Hot Springs) located in two different basins presenting marine sediments of the Cretaceous period (Late Albian and Cenomanian–Turonian, respectively), that were deposited in shallow epicontinental seas, from sections presenting different facies (Fig. 1A).

2.1. Section of Wissant (Albian, Boulonnais, North of France)

The studied outcrop, located at Wissant (Cap Blanc Nez cliff) in the northern part of the Paris Basin, exhibits Albian to Cenomanian sediments. These sediments were deposited in an epicontinental sea close to the western part of the Rhenish Massif (i.e. London-Brabant area), which was the likely source of detrital particles (Robaszynski and Amédro, 1993). This area was located within a marine pathway between the Boreal and Tethyan realms (Fig. 1B). The sedimentary succession consists of three formations: the Gardes formation composed of green glauconitic sandstones (Early Albian), the Saint Pô formation composed of dark-grey claystones alternating with common horizons of phosphatic nodules and pyritized macrofauna (Middle and Upper Albian), and the Strouanne formation composed of bioturbated glauconitic chalk (Early Cenomanian, Robaszynski et al., 1980) (Fig. 2A). Sediment contains abundant bivalves, gasteropods, ammonites, scaphopods, echinoderms and both benthic and planktonic foraminifers. The main planktonic foraminifera are *Globigerinelloides*, *Hedbergella*, *Guembelitria*, and *Heterohelix*. The abundance of planktonic foraminifera indicates an open marine environment, that is also supported by the large diversity of the invertebrate fauna. Amongst benthic foraminifera, the dominant genus is *Gavelinella*, associated with abundant *Epistomina* and *Hoeglundina*. The abundant benthic foraminifers, gastropods, and bivalves indicate oxic conditions at the seafloor. The foraminifera associations point to a moderate to low energy environment. The absence of wave-induced sedimentary structures indicates that the sediment was deposited below tidal and probably storm wave base (Knight, 1997), in lower offshore palaeoenvironments (Robaszynski et al., 1980). A maximum depth of 100–350 m can be inferred for this section (Khan, 1950; Knight, 1997). The highly condensed nature of this section and the overall low sedimentation rate (about 11 m for the whole Albian stage), is expressed by the occurrence of phosphatic beds. These phosphatic beds have been interpreted as resulting from upwellings that developed during a marine transgression (Amédro, 1992). The sedimentary succession records fluctuations of sea-level as well as tectonic rejuvenations of the London-Brabant Massif (Robaszynski and Amédro, 1993). The different fractions analyzed in this work have been sampled in the dark-grey claystones of the Saint Pô formation (Upper Albian, Fig. 2A), except for one level sampled in the phosphatic horizon 6.

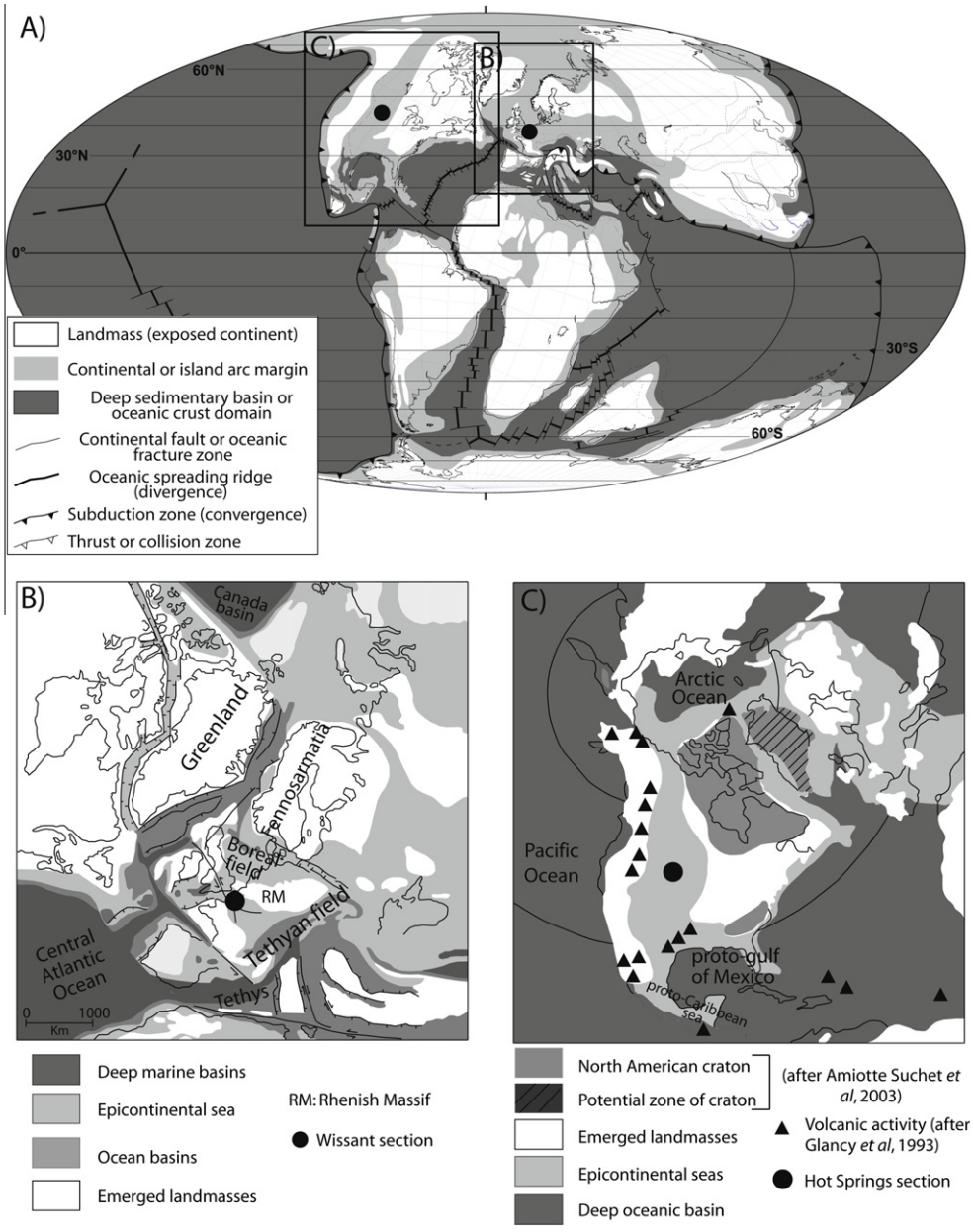

Fig. 1. Location of the studied sections on (A) a wordwide palaeogeographic map of the Middle Cretaceous (Vrielynck and Bouysse, 2003), (B) a paleogeographic map of the NW Tethys during the Albian period (modified from Ziegler, 1990), and (C) a paleogeographic map of North America during the Cenomanian–Turonian period (modified from Hay et al., 1993).

2.2. Section of Hot Springs (Cenomanian–Turonian stage boundary, South Dakota, USA)

During the Jurassic-Cretaceous period, the combination of subsidence and tectono-eustatic highstand has led to the establishment of the Western Interior Basin (WIB), an elongated foreland marine basin (Kauffman, 1977; Hay et al., 1993) developed between the north American Cordilleran orogenic belt (Sevier Highlands) (Weimer, 1984; Jordan, 1991) and the north American craton (Caldwell and Kauffman, 1993) (Fig. 1C). At the time of maximum Cretaceous transgression, this epicontinental seaway was about 2000 km wide and extended 6000 km through the middle of North America linking the boreal realm to the Gulf of Mexico (Kauffman, 1977; Caldwell and Kauffman, 1993; Hay et al., 1993; Fig. 1C). In its deepest parts, the basin depth could have reached 200 to 500 m, according to Asquith (1970), Batt (1987), and Sageman and Arthur (1994).

The outcrop is located close to Hot Springs (South Dakota, USA) and exhibits Cenomanian–Turonian sediments. The hemipelagic sedimentary succession (Fig. 2B), equivalent of the more southerly Bridge Creek Member of the Greenhorn Formation, is composed of rhythmically bedded prominent limestone beds alternating with dark-grey

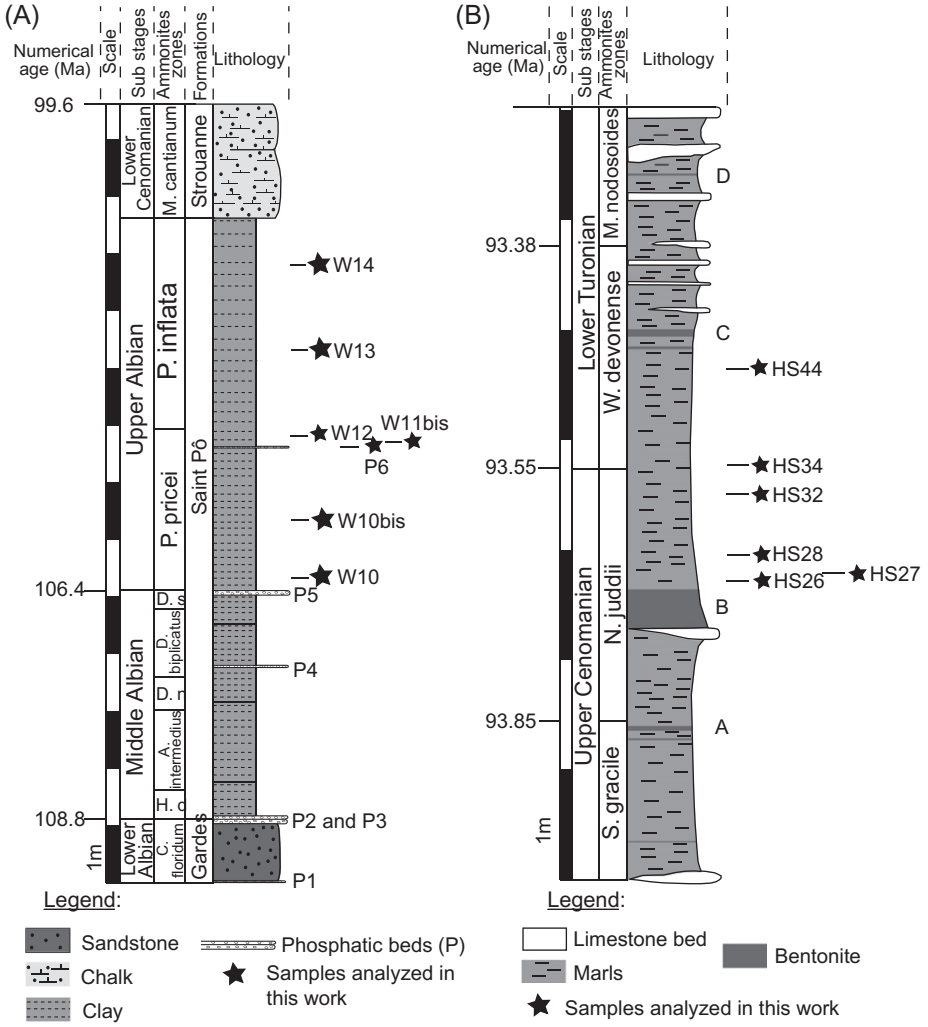

Fig. 2. A. Litho, bio and chronostratigraphy of the Wissant section (North France) (modified from Robaszynski et al., 1980) and distribution of the sampled levels on the section. Ammonite zones are from Amédro (1992), numerical ages are derived from the time scale of Gradstein et al. (2004). B. Litho-, bio- and chronostratigraphy of the Cenomanian–Turonian boundary interval, at the section of Hot Springs (South Dakota) (modified from Desmares, 2005). Ammonite zones and identification of major bentonite marker beds are from Elder (1987). Absolute ages derived from the time scale of Gradstein et al. (2004). Numerical ages are derived from the orbital time scale estimated at Pueblo by Sageman et al. (2006).

marlstone/calcareous shales (Desmares, 2005) interrupted by five major altered ash layers (bentonites designed as A, B, C, D and E; Elder, 1987; Desmares et al., 2007). Six levels were sampled between bentonites B and C (Fig. 2B). The sampled interval includes the Cenomanian–Turonian boundary and coincides with the acme of the oceanic anoxic event (OAE2) as expressed by the distinctive second positive $\delta^{13}C$ shift and plateau (Desmares et al., 2007). Detailed thin section analysis reveals that the microfacies of the studied samples are characterized by organic carbon-rich laminae (Fig. 3). The presence of planktonic foraminifera and ammonites argue for open marine conditions, in agreement with other works (Eicher and Diner, 1989). Planktonic foraminifera are not diverse with a predominance of inflated forms such as *Whiteinella* and *Hedbergella* which evolved in surface and intermediate waters. Associated with such microfacies, the absence of deepest-dwelling

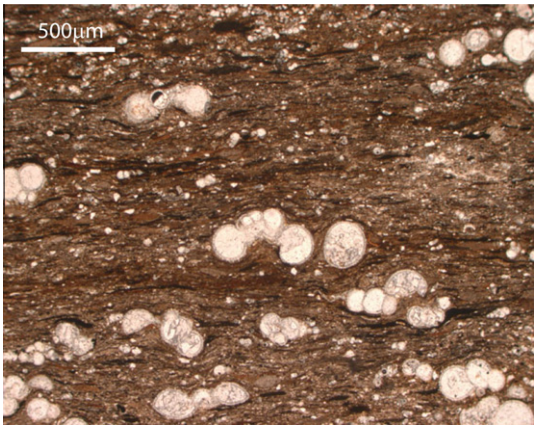

Fig. 3. Anoxic microfacies showing organic matter-rich laminae and inflated planktonic foraminifera at Hot Spring, level HS27.

keeled morphotypes and of benthic foraminifera points to oxygen-poor conditions in bottom waters.

Based on the cyclostratigraphic analysis of Sageman et al. (2006) in the Pueblo type section, the time interval between the bentonites B and C could represent around 287 ky, indicating a quite low sedimentation rate in Hot Springs (0.8 cm/ky). The different fractions analyzed have been sampled in marlstone beds (Fig. 2B).

3. ANALYTICAL PROCEDURE

Fish teeth (about 0.2–2.0 mg) and mixed planktonic foraminifera (between ~8.3 to 17.3 mg) fractions were handpicked from the >125 μm fraction of desagregated sediments. At Wissant, wet sieving of sediments was sufficient to desagregate the sediments and isolate the foraminifera tests. The samples at Hot Spring have been recovered in the marl interbeds, that were not much lithified and from which the foraminifera were easily extracted through soaking in dilute oxygen peroxide (0.2%) for 24 h before sieving. Fossil fish teeth were cleaned in ultrasonic bath and dissolved in twice-suboiled concentrated HCl, after addition of 100 μL T_m spike (about 8 ng T_m). Part of the foraminifera samples were directly dissolved in 4 M HCl. These samples are referred to as "foraminifera" in Table 1 and in the remainder of the paper. To prevent any contamination from detrital phases that may have occurred with dissolution in 4 M HCl, the other part of the foraminifera samples were dissolved at room temperature using a mixed 0.05 M hydroxylamine hydrochloride (HH) and 15% v/v acetic acid (AA) solution (referred to as "HH-extraction of foraminifera" from here on). About 300 mg of bulk sediments were treated with dilute acetic acid solution (2% v/v) to remove carbonates. Then, the Fe–Mn oxyhydroxide fractions of the decarbonated sediment samples were extracted with 0.05 M HH and 15% AA ("sediment HH extraction"), following Bayon et al. (2002). The residual detrital phases left after the sequential leaching procedure were digested by alkaline fusion (Bayon et al., 2009). Trace element abundances in all these different fractions (fish teeth, HH extraction of foraminifera, foraminifera, and detrital fraction) except sediment HH-extractions were determined at the Pôle Spectrométrie Océan (PSO, Brest, France) on an Element 2 inductively coupled plasma-sector field mass spectrometer (ICP-SFMS, Thermo Fisher Scientific) (Table 2). The REE were analyzed with the low resolution mode, but were corrected for oxide and hydroxide interferences by analyzing solutions of ultra-pure water, Ba + Ce, Pr + Nd and Sm + Gd + Tb (Barrat et al., 1996; Bayon et al., 2009). Elemental concentrations in the studied samples were calculated using the T_m addition method (Barrat et al., 1996), which was validated recently for the analysis of both sediment (Bayon et al., 2009) and carbonate samples (Rongemaille et al., 2011). With this method, the raw data acquired during the measurement session are calibrated against an unspiked (no added T_m) BHVO-2 reference solution, run after every three samples to correct for the instrumental drift. Elemental concentrations are then calculated using the sample mass and the amount of T_m added. The BHVO-2 values used for the calculations are given in Barrat et al. (2012). Details on the method can be found in Bayon et al. (2009).

Prior to the isotopic analyses, Nd fractions were isolated using standard ion exchange techniques. The REE were first separated in 4-M HCl using polypropylene columns containing Bio-Rad AG50W-X8 resin. Neodymium was separated from the other REE in 0.25 M HCl with columns containing Ln resin (Eichrom), based on a method developed by Pin and Zalduegui (1997).

Nd isotope measurements were performed at the PSO (Brest, France) on a Neptune multi-collector inductively coupled plasma mass spectrometer (MC-ICP-MS, Thermo Fisher Scientific). Nd isotope ratios were corrected for mass discrimination by normalizing to $^{146}Nd/^{144}Nd = 0.7219$ using an exponential law. The corrected isotopic ratios were normalized to $^{143}Nd/^{144}Nd = 0.511858$ for the La Jolla Nd standard. Analyses of the JNdi-1 standard gave $^{143}Nd/^{144}Nd$ of 0.512114 ± 0.000011 (2 s.d., $n = 5$), which corresponds to an external reproducibility of $\sim 0.21\varepsilon$. Nd blanks were typically less than 300 pg and hence usually negligible relative to the Nd signals measured in this study.

All $^{143}Nd/^{144}Nd$ values analyzed on the MC-ICP-MS were reported in Table 1. The Nd isotopic ratios were expressed with the epsilon notation (ε_{Nd}), corrected for the radioactive decay of ^{147}Sm to ^{143}Nd using the Nd and Sm concentrations determined for the same samples, presented in Table 2 ($^{147}Sm/^{144}Nd = Sm/Nd * 0.6049$), the stratigraphic age (t) of the studied sedimentary units, and the ^{147}Sm radioactive decay constant λ (6.54×10^{-12}; Lugmair and Marti, 1977) (Table 1). For sediment HH-extraction samples, a $^{147}Sm/^{144}Nd$ value of 0.129 was assumed (Martin et al., 2010), as the trace element abundances of these samples were not determined. This value is quite close to the average $^{147}Sm/^{144}Nd$ calculated for the HH-extraction phase of foraminifera in our study (0.124). The difference in calculated $\varepsilon_{Nd(t)}$ values using the lowest (0.123) and the highest (0.136) $^{147}Sm/^{144}Nd$ measured by Martin et al. (2010) in marine sediment HH-extraction is less than 0.2 ε-units and thus less than the external reproducibility. The CHUR $^{143}Nd/^{144}Nd$ ratio was corrected for post-sedimentation decay of ^{147}Sm using a present-day value of 0.512638 and a $^{147}Sm/^{144}Nd$ ratio of 0.1967 (Jacobsen and Wasserburg, 1980).

4. RESULTS

4.1. REE patterns

For the two studied sites, the detrital fractions display a flat shale-normalized REE pattern (i.e. typical of shales; Fig. 4). In contrast, the REE patterns recorded by the other studied fractions are different between the two studied sections. At Wissant, HH-extraction of foraminifera, foraminifera, and fish teeth all record an enrichment in Middle Rare Earth Elements (MREE bulge pattern) and a positive cerium (Ce) anomaly (Fig. 4A). At Hot Spring, the fish teeth record a similar MREE bulge pattern, but HH-extraction of foraminifera and foraminifera exhibit a clearly different pattern, marked by a strong enrichment of Heavy Rare Earth Elements (HREE) (Fig. 4B). No cerium anomaly is recorded

Table 1
Description, location, ages and Nd compositions of samples analyzed in this work.

Samples	Location	Stratigraphic age	Age (Ma)[a]	Fish teeth				Foraminifera				HH extraction of foraminifera			
				$^{143}Nd/^{144}Nd$	2σ	$\varepsilon_{Nd(t)}$[b]	2σ	$^{143}Nd/^{144}Nd$	2σ	$\varepsilon_{Nd(t)}$	2σ	$^{143}Nd/^{144}Nd$	2σ	$\varepsilon_{Nd(t)}$	2σ
W10	Wissant	Late Albian	106.3	0.512121	0.000004	−9.22	0.08	–	–	–	–	–	–	–	–
W10bis	Wissant	Late Albian	105.5	0.512152	0.000004	−8.61	0.08	0.512135	0.000005	−8.86	0.10	0.512149	0.000006	−8.55	0.12
P6	Wissant	Late Albian	104.5	0.512099	0.000005	−9.57	0.10	0.512079	0.000007	−9.89	0.13	–	–	–	–
W11bis	Wissant	Late Albian	104.3	0.512124	0.000004	−9.16	0.08	0.512109	0.000004	−9.35	0.08	–	–	–	–
W12	Wissant	Late Albian	104.2	0.512185	0.000005	−7.86	0.10	0.512091	0.000006	−9.73	0.12	–	–	–	–
W13	Wissant	Late Albian	103.0	0.512114	0.000004	−9.39	0.08	0.512111	0.00001	−9.35	0.20	0.512105	0.000008	−9.43	0.15
W14	Wissant	Late Albian	101.8	0.512158	0.000004	−8.65	0.08	–	–	–	–	–	–	–	–
HS26	Hot Springs	Late Cenomanian	93.69	0.512243	0.000004	−6.90	0.08	0.512236	0.000005	−6.91	0.10	0.512244	0.000006	−6.75	0.12
HS27	Hot Springs	Late Cenomanian	93.68	0.512251	0.000005	−6.72	0.10	0.512260	0.000004	−6.65	0.08	0.512277	0.000008	−6.30	0.15
HS28	Hot Springs	Late Cenomanian	93.65	0.512285	0.000005	−5.95	0.10	0.512287	0.000011	−6.05	0.21	–	–	–	–
HS32	Hot Springs	Late Cenomanian	93.58	0.512276	0.000005	−6.20	0.10	–	–	–	–	–	–	–	–
HS34	Hot Springs	Early Turonian	93.55	0.512281	0.000007	−6.11	0.15	–	–	–	–	–	–	–	–
HS44	Hot Springs	Early Turonian	93.47	0.512280	0.000007	−6.07	0.14	–	–	–	–	–	–	–	–

Samples	Location	Stratigraphic age	Age (Ma)[a]	HH extraction of bulk sediment				Bulk sediment			
				$^{143}Nd/^{144}Nd$	2σ	$\varepsilon_{Nd(t)}$	2σ	$^{143}Nd/^{144}Nd$	2σ	$\varepsilon_{Nd(t)}$	2σ
W10	Wissant	Late Albian	106.3	–	–	–	–	0.512004	0.000006	−11.16	0.12
W10bis	Wissant	Late Albian	105.5	0.512139	0.000007	−8.83	0.13	0.512093	0.000007	−9.52	0.13
P6	Wissant	Late Albian	104.5	0.512059	0.000005	−10.39	0.10	0.511993	0.000005	−11.42	0.10
W14	Wissant	Late Albian	101.8	–	–	–	–	0.512049	0.000005	−10.34	0.09
HS27	Hot Springs	Late Cenomanian	93.68	0.512239	0.000007	−6.98	0.13	0.512100	0.000007	−9.46	0.13
HS32	Hot Springs	Late Cenomanian	93.58	0.512241	0.000005	−6.94	0.10	0.512099	0.000005	−9.42	0.09
HS34	Hot Springs	Early Turonian	93.55	0.512246	0.000006	−6.85	0.12	0.512078	0.000005	−9.78	0.10
HS44	Hot Springs	Early Turonian	93.47	0.512264	0.000005	−6.48	0.10	0.512069	0.000005	−9.97	0.10

[a]Absolute ages are derived from the time scale of Gradstein et al. (2004) for Wissant and Sageman et al. (2006) for Hot Springs.
[b]See text (part 3. Analytical procedure) for details of $\varepsilon_{Nd(t)}$ calculation.

Table 2
REE values in ppm for fish teeth. foraminifera. HH extraction of foraminifera and detrital fraction.

Sample	La ppm	Ce ppm	Pr ppm	Nd ppm	Sm ppm	Eu ppm	Gd ppm	Tb ppm	Dy ppm	Ho ppm	Er ppm	Yb ppm	Lu ppm
Fish teeth													
W10	617.70	3496.10	279.33	1153.50	251.86	48.13	186.23	25.06	119.61	19.56	46.45	21.12	2.65
W10bis	59.80	326.24	30.76	129.70	28.36	5.48	21.93	2.87	13.53	2.21	4.74	2.48	0.32
P6	65.31	277.17	26.72	106.99	22.28	4.76	19.40	2.61	12.90	2.24	5.01	2.66	0.33
W11bis	68.34	332.86	32.34	134.04	29.16	5.72	23.19	3.00	14.19	2.32	5.03	2.72	0.34
W12	59.88	321.88	28.52	113.13	23.05	4.73	17.17	2.19	10.09	1.64	3.59	1.95	0.23
W13	125.73	643.30	60.92	254.41	56.09	11.31	44.51	5.86	27.97	4.67	10.18	5.41	0.68
W14	1365.48	7652.49	807.29	3538.92	829.24	150.81	610.99	79.29	365.52	56.29	124.06	49.12	6.06
HS26	610.22	1326.52	263.68	1037.69	222.32	27.38	172.69	21.26	95.14	14.86	30.96	17.23	1.91
HS27	422.52	1160.56	162.98	655.46	137.64	18.14	115.43	14.44	66.88	10.65	22.89	12.40	1.47
HS28	737.20	2001.55	286.49	1121.34	220.10	36.00	189.15	23.05	109.06	18.62	39.59	20.39	2.50
HS32	2381.96	5857.45	806.01	3288.40	674.02	124.67	605.91	80.45	427.90	74.01	173.17	79.82	9.83
HS34	1329.69	3236.75	449.28	1812.32	375.70	72.34	343.25	46.58	253.46	45.36	108.37	55.64	7.05
HS44	1377.07	2975.86	417.97	1702.88	337.51	65.57	319.26	41.15	222.50	39.66	95.05	45.04	5.52
Foraminifera													
W10bis	12.68	42.85	3.19	11.41	2.37	0.54	2.16	0.34	1.89	0.36	0.94	0.72	0.10
P6	15.10	42.12	3.32	11.90	2.37	0.55	2.41	0.36	1.99	0.39	1.02	0.78	0.11
W11bis	12.50	38.75	3.04	11.06	2.26	0.50	1.97	0.31	1.71	0.33	0.86	0.66	0.09
W12	15.86	48.26	4.03	14.76	3.07	0.71	2.92	0.46	2.50	0.48	1.21	0.90	0.12
W13	16.65	53.31	4.00	14.30	2.98	0.69	2.65	0.42	2.36	0.45	1.16	0.87	0.13
HS26	37.51	40.58	6.14	20.34	3.99	0.77	4.53	0.89	6.47	1.56	5.02	5.59	0.82
HS27	25.87	42.16	4.36	14.43	3.24	0.66	3.80	0.77	5.54	1.32	4.26	4.62	0.69
HS28	14.12	27.23	3.11	10.49	2.26	0.48	2.34	0.46	3.14	0.72	2.24	2.68	0.40
HH extraction of foraminifera													
W10bis	32.74	111.83	8.17	29.28	5.94	1.35	5.09	0.87	4.90	0.94	2.48	1.91	0.26
W13	27.90	87.67	6.56	23.63	4.79	1.08	4.09	0.68	3.82	0.74	1.93	1.47	0.20
HS26	51.66	55.67	8.29	27.73	5.41	1.04	6.17	1.24	9.10	2.19	6.97	7.78	1.13
HS27	48.62	78.89	8.30	27.87	6.19	1.23	7.18	1.52	11.06	2.60	8.12	8.94	1.29
Detrital fraction													
W10	18.35	36.59	4.06	14.45	2.56	0.60	2.00	0.35	2.18	0.45	1.37	1.34	0.18
W10bis	23.25	60.03	5.78	20.92	3.94	0.86	3.09	0.54	3.16	0.63	1.81	1.62	0.21
P6	34.05	71.27	7.64	27.52	4.97	1.01	4.43	0.68	4.09	0.86	2.50	2.60	0.38
W14	16.08	33.48	3.61	12.73	2.29	0.49	1.79	0.32	1.99	0.41	1.23	1.19	0.15
HS27	32.58	56.66	6.61	23.53	4.29	0.71	4.02	0.61	3.64	0.74	2.11	2.09	0.29
HS32	15.19	28.87	3.26	11.42	1.96	0.45	1.53	0.26	1.65	0.35	1.07	1.05	0.14
HS34	20.23	35.00	4.03	14.01	2.34	0.55	1.79	0.31	1.98	0.43	1.30	1.25	0.16
HS44	26.97	45.54	5.27	18.48	3.11	0.70	2.47	0.41	2.54	0.55	1.64	1.54	0.19

in the different REE patterns in the Hot Spring material, except for sample HS26 for which a weakly negative Ce anomaly is recorded in all phases (HH-extraction of foraminifera, foraminifera, and fish teeth).

4.2. $\varepsilon_{Nd(t)}$ values of different materials and sections

For both sites, the detrital fraction yields systematically the least radiogenic $\varepsilon_{Nd(t)}$ values (Fig. 5). At Wissant, these values are quite variable and range from −11.4 to −9.5 initial ε-units (Fig. 5A). At Hot springs, $\varepsilon_{Nd(t)}$ values of the detrital fraction remain in a smaller range, with two samples from the Late Cenomanian yielding a $\varepsilon_{Nd(t)}$ around −9.4 and two samples from the Early Turonian yielding more negative $\varepsilon_{Nd(t)}$ values of −9.8 and −10.0 (Fig. 5B). Fish tooth $\varepsilon_{Nd(t)}$ values are markedly more radiogenic in both sections, with values ranging between −7.9 and −9.6 at Wissant (Fig. 5A) and between −5.9 and −6.9 at Hot Springs (Fig. 5B). At Wissant, although the difference between the Nd isotopic composition of the detrital fraction and fish teeth is variable and based on only 4 levels, the $\varepsilon_{Nd(t)}$ values of fish teeth and of the detrital fraction seem to be linked, with fish teeth $\varepsilon_{Nd(t)}$ being higher in levels of higher $\varepsilon_{Nd(t)}$ of the detrital fraction, and lower in levels of lower $\varepsilon_{Nd(t)}$ of the detrital fraction.

With the exception of one sample (W12), the $\varepsilon_{Nd(t)}$ values of both HH-extraction of foraminifera and of foraminifera tests are close to that of fish teeth (0.15 ε-units of difference on average, but up to 0.4 ε-units) for both sites (Fig. 5, Fig. 6). Foraminifera tend to yield slightly more negative $\varepsilon_{Nd(t)}$ values, and HH-extraction of foraminifera slightly less negative $\varepsilon_{Nd(t)}$ values than that of fish teeth. In contrast, sediment HH-extractions exhibit $\varepsilon_{Nd(t)}$ values that are intermediate between that of fish teeth and of the detrital fraction, although closer to the composition of fish teeth (Fig. 5; Fig. 6). The difference of sediment HH-extraction

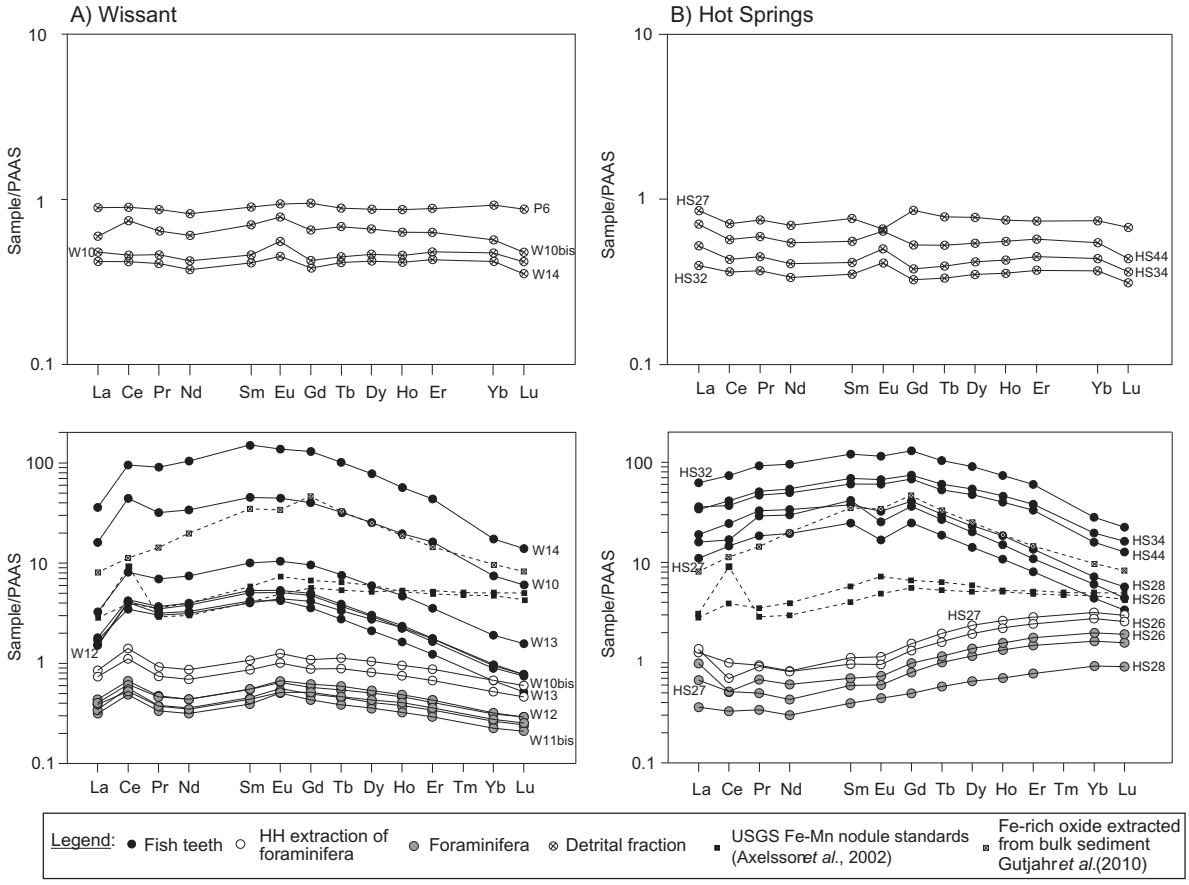

Fig. 4. Rare earth element (REE) patterns for the detrital fraction (crossed circles), for fossil fish teeth (black circles), for foraminifera (grey circles), and for HH chemical extractions of foraminifera (white circles) normalized to Post-Archean Australian Shale (PAAS, Taylor and McLennan, 1985), from (A) Wissant, (B) Hot Spring. REE spectra of the standards manganese nodules NOD-A-1 and NOD-P-1 normalized to PAAS are shown for comparison (data from Axelsson et al., 2002), along with an Fe-rich oxide PAAS-normalized REE spectra (average of all analyzed Fe–Mn spectra from Gutjahr et al., 2010).

$\varepsilon_{Nd(t)}$ values with that of fish teeth is variable, ranging from 0.22 to 0.82 ε-units (Fig. 6). Note that because not all phases have been measured in all levels, these observations are based on only 4 to 8 levels, depending on the fraction considered.

5. DISCUSSION

5.1. REE patterns

In order to compare the different REE patterns observed in this work with those from the literature, we calculated shale-normalized ratios: HREE/LREE and MREE/MREE*, where HREE represents the sum of the PAAS-normalized concentrations of T_m, Yb, and Lu, LREE the sum of the concentrations of La, Pr, and Nd, MREE the sum of the concentrations of Gd, Tb, and Dy, and MREE* the average of HREE and LREE (Martin et al., 2010, modified from Haley et al., 2004) (Fig. 7). Because T_m has not been measured in this work, $(T_m)N$ concentrations were estimated by $(Er + Yb)N/2$. The MREE/MREE* ratio allows quantification of the extent of the MREE bulge in REE patterns, and HREE/LREE allows quantification of the HREE enrichment over LREE.

5.1.1. Wissant section

At Wissant, the MREE bulge-type profiles displayed by both HH-extraction of foraminifera and foraminifera are typical of mixed Fe–Mn oxyhydroxide coating patterns, which can exhibit variable Ce anomalies (Axelsson et al., 2002; Bayon et al., 2002; Gutjahr et al., 2007; Martin et al., 2010) (Figs. 4A and 7). This observation suggests that oxides dominate the REE signal over calcite in foraminiferal tests, which is coherent with the low REE concentrations recorded in biogenic carbonates relative to the higher concentrations recorded in Fe–Mn oxides (Palmer, 1985; Axelsson et al., 2002; Gourlan, 2006; Gourlan et al., 2010; Roberts et al., 2010).

The foraminifera chambers were not broken up and ultrasonicated prior to dissolution to remove possibly present intratest clays or other contaminant phases. It could therefore be argued that for foraminifera dissolved in 4 M HCl, a MREE bulge-type profile may reflect a mixed signal of an authigenic phase with even stronger MREE enrichment and some contribution from a terrigenous phase that may have been present within the chambers and partially leached by the 4 M HCl solution. Yet if this was indeed the case, we would have expected different spectra from the extracted foraminifera Fe–Mn oxyhydroxide phase, that are on the

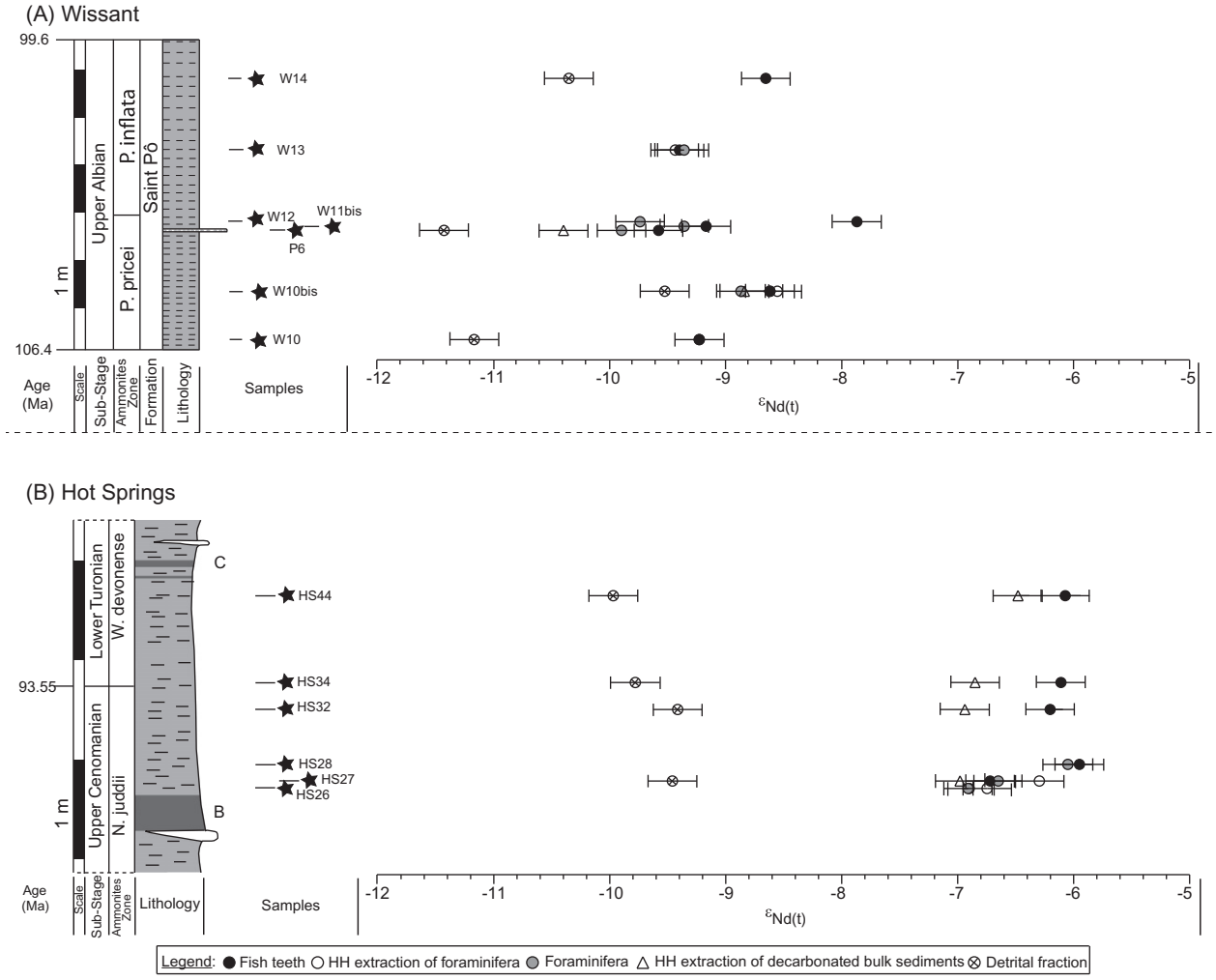

Fig. 5. Evolution of the Nd isotopes compositions of fossil fish teeth (black circles), HH extraction of foraminifera (white circles), foraminifera (gray circles), HH extraction of bulk sediment (white triangles), detrital fraction (crossed circles) measures in this study along the two studied sections, Wissant (A) and Hot Springs (B).

contrary undistinguishable from that of the foraminifera dissolved in 4 M HCl (Fig. 4). This similarity along with the good agreement of the Nd isotope values of both phases (foraminifera tests dissolved in 4 M HCl and leached foraminifera tests) suggest that there is no major contribution from any residual detrital material in the foraminifera dissolved in 4 M HCl. In addition, if a detrital contamination of the samples had occurred, we would expect the samples presenting an ε_{Nd} value closer to that of the detrital fraction to also present a flatter REE spectra, represented by lower MREE/MREE* values. Although the data are not numerous, because the detrital fraction has not been analyzed in every level, the plotted data do not show any relation between MREE/MREE* and the difference of ε_{Nd} between the detrital fraction and the other phases (Fig. 8). Again, this argues for the absence of any significant detrital contamination of the foraminifera and HH-extraction of foraminifera, as well as of fish teeth.

Although they present a slightly stronger MREE enrichment, and a slightly lower HREE enrichment, fish tooth REE patterns remain quite similar to those of Fe–Mn oxides (Figs. 4A and 7), and this is in agreement with previous studies (Elderfield and Pagett, 1986; Martin et al., 2010). It is furthermore notable that REE patterns with only small HREE enrichments were also reported for Fe-rich oxides, which were characterized by high (Fe/Mn) ratios (Gutjahr et al., 2010; Fig. 4). In this study, the fish tooth samples were not reductively cleaned prior to dissolution. Yet because of the strong enrichment of REEs in apatite (typically several hundreds to several thousands of ppm; e.g. Martin et al., 2010), modification of the REE composition of the fish teeth would require a very large proportion of Fe–Mn oxides coating the teeth. In addition, the REE patterns of our fish teeth are indistinguishable from those of fish remains having undergone the oxidative/reductive cleaning designed to remove Fe–Mn oxide coatings (e.g. Martin et al., 2010). This suggests that the MREE-bulge profile observed in our study is likely a feature of apatite rather than representing an influence of REEs from potential oxide coatings.

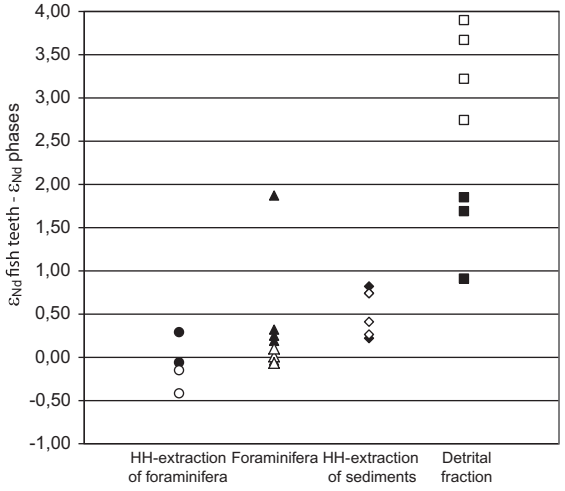

Fig. 6. Difference of Nd isotope composition between fish teeth and that of the different phases: HH-extraction of foraminifera (circles), foraminifera (triangles), HH-extraction of sediments (diamonds), and detrital fraction (squares) at Wissant (black) and Hot Spring (white).

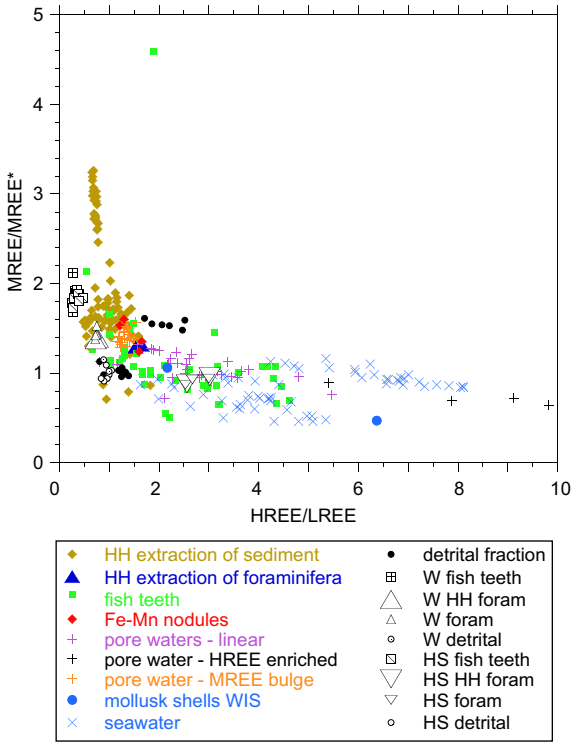

Fig. 7. Comparison of PAAS normalized HREE/LREE (T_m + Yb + Lu)/(La + Pr + Nd) vs. MREE/MREE* (Gd + Tb + Dy/average of HREE and LREE) of fossil fish teeth, HH extraction of foraminifera, foraminifera and detrital fraction measured in this study with that of different archives available in the literature. Data from literature: HH extraction of bulk sediments are from Bayon et al. (2002, 2004), Gutjahr et al. (2007), Gutjahr et al. (2010), Martin et al. (2010), and Basak et al. (2011); HH extraction of foraminifera are from Bayon et al. (2004); fish teeth are from Grandjean et al. (1987), Picard et al. (2002), and Martin et al. (2010); Fe–Mn nodules are from Axelsson et al. (2002) and Gutjahr et al. (2010); pore water are from Elderfield and Sholkovitz (1987) and Haley et al. (2004); mollusks shells are from Whittaker and Kyser (1993); modern seawater are from De Baar et al. (1985), Piepgras and Jacobsen (1992), Arraes-Mescoff et al. (2001), Lacan and Jeandel (2005a), and Zhang et al. (2008); and detrital fraction are from Elderfield and Sholkovitz (1987), Bayon et al. (2002), and Gutjahr et al. (2007).

It can be noted that various REE spectra have been reported from fish teeth, from MREE-bulge profiles to spectra that are similar to that of seawater (Elderfield and Pagett, 1986; Grandjean et al., 1987; Picard et al., 2002; Martin et al., 2010) (Fig. 7). The amount of REE in living fish teeth is negligible, and an MREE bulge in fossil fish apatite therefore derives from diagenetic incorporation of REEs. Thermodynamic considerations predict that this incorporation can take place (1) with a preferential intake of MREEs through substitution, (2) with little fractionation of the lanthanide series through adsorption, or (3) by a combination of the two processes (Koeppenkastrop and De Carlo, 1992; Reynard et al., 1999). Therefore, a bulge MREE profile in the fish teeth from Wissant can either reflect REE incorporation from a medium that has a REE profile typical of seawater, enriched in HREEs, if the substitution process is dominant, or, if the absorption process dominates, from a medium that present a bulge MREE profile already, that can derive for instance from dissolution of Fe–Mn oxides (Haley et al., 2004).

5.1.2. Hot Springs section

Similarly to the Wissant section, the REE profiles of foraminifera are identical to that of HH-extraction of foraminifera in the HS26 and HS27 levels where both fractions have been analyzed (Fig. 4B). However, these REE profiles do not record MREE bulge patterns typical of Fe–Mn oxides but are characterized by a greater enrichment in HREE instead (Fig. 4B and Fig. 7). These profiles are similar to those of REE integrated in calcite from seawater (Elderfield et al., 1981; Palmer, 1985; Schields and Webb, 2004; Haley et al., 2005), without the Ce anomaly except for sample HS26. These REE patterns, including the absence of Ce anomaly, are similar to that recorded by mollusk shells from a nearby location and age, that has been interpreted to reflect the composition of local seawater (Whittaker and Kyser, 1993) (Fig. 7). In contrast, the fish tooth shale-normalized REE patterns are comparable to those observed for the Wissant section samples (Fig. 4B), with the exception of the positive Ce anomaly that is absent at Hot Springs. Similarly to the Wissant samples, there is no evident relation between MREE/MREE* or HREE/LREE and the difference of ε_{Nd} between the detrital fraction and the other phases (Fig. 8). In addition, the comparable REE spectra of foraminifera tests dissolved in 4 M HCl and of leached foraminifera tests along with the good agreement of the Nd isotope values of both phases argues for the absence of any significant detrital contamination of the foraminifera and HH-extraction of foraminifera at Hot Spring as well.

The lack of preferential MREE enrichment in the HH-extraction of foraminifera, along with the precense of this

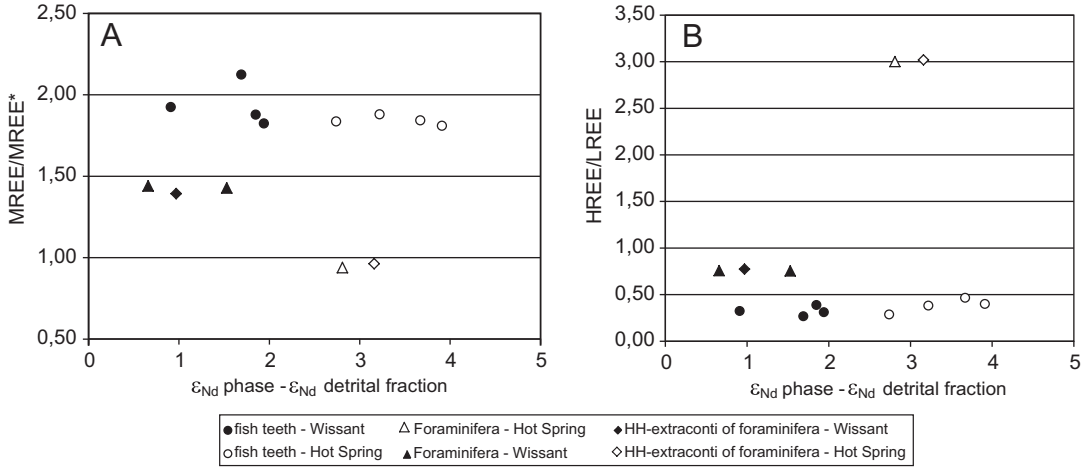

Fig. 8. Relation between the MREE/MREE* (A) and HREE/LREE (B) with the difference of ε_{Nd} between the different phases and the detrital fraction at Wissant and at Hot Spring.

preferential MREE enrichment in fish teeth, could be explained by a migration of a late diagenetic front through the sedimentary column that may have remobilized a significant fraction of previously present Fe–Mn oxyhydroxides. Alternatively, this lack of preferential MREE enrichment in the HH-extraction of foraminifera may also be explained by an absence of oxide formation at Hot Springs during the studied interval. Indeed, despite the absence of black-shales in the Western Interior Basin, the sampled interval between bentonites B and C is coeval to the acme of Oceanic Anoxic Event 2 (OAE2 e.g. Arthur et al., 1987, 1988), and dysoxic to anoxic benthic conditions have been inferred across wide areas of the seaway (Leckie et al., 1998). At Hot Spring, both microfacies that show organic-rich carbon laminae, and the absence of deepest-dwelling keeled morphotypes and of benthic foraminifera point to oxygen-poor conditions at this location as well. As a result, formation of authigenic Fe–Mn oxyhydroxide phases may then have been hindered. It has been recently suggested that intratest organic matter could be an important carrier of Nd in foraminifera (Vance et al., 2004; Martinez-Boti et al., 2009). Haley et al. (2004) has shown that pore waters with a "linear" pattern (Fig. 7), described as a constant but moderate increase in the PAAS-normalized REEs across the series, reflected release of REEs from organic matters into pore waters. The HREE/LREE and MREE/MREE* ratios calculated from REE concentrations of foraminifera and HH-extraction of foraminifera at Hot Springs plot within the domain defined by this "linear" REE profile measured in pore waters by Haley et al. (2004) (Fig. 7). If dysoxic or anoxic conditions have indeed occurred at Hot Spring, as suggested by the microfacies and absence of benthic foraminifera, it is difficult to think that REEs could have been released into pore waters through oxidation of organic matter. However, anoxic conditions may have favored the preservation of intratest organic matter within the foraminifera tests, that could have been analyzed along with calcite in this study.

The absence of a negative Ce anomaly in the REE patterns recorded at Hot Springs may also point toward anoxic conditions, although it has been emphasized that interpretation of the Ce anomaly should be taken with great care (German and Elderfield, 1990; Haley et al., 2004). In addition, a weakly negative or even positive Ce anomaly may also be a feature of proximal shelf environments (Elderfield and Pagett, 1986; Elderfield et al., 1990). If the absence of a Ce anomaly reflects anoxia at Hot Spring, then the weakly negative Ce anomaly recorded in sample HS26, both in the HH-extraction of foraminifera, in foraminifera, and in fish teeth, may indicate sporadic interruption of anoxia within the studied interval.

In either case, remobilization of previously present Fe–Mn oxides or initial absence of Fe–Mn oxide formation due to oxygen-poor bottom water conditions, the similar REE profiles in fish teeth recorded at Wissant and at Hot Spring supports the interpretation that the REEs in the fish teeth analyzed in this study are located in apatite rather than in potential Fe–Mn oxides coated on the teeth. If the second hypothesis, that marine authigenic Fe–Mn oxides did not form in this environment, is correct, the MREE bulge pattern recorded by fish tooth apatite would support a preferential integration of MREE from bottom water through substitution during early diagenesis. This interpretation follows that of Martin et al. (2010) rather than a quantitative integration of REEs from pore waters with a bulge MREE profile deriving from dissolution of Fe–Mn oxides.

5.2. Nd isotope compositions

5.2.1. Significance of the $\varepsilon_{Nd(t)}$ of planktonic foraminifera and of their Fe–Mn oxide coatings in the studied shelf environments

Both at Wissant and at Hot Spring, the foraminifera and HH-extraction of foraminifera record Nd isotope compositions similar to that of contemporaneous fish teeth (Figs. 5 and 6). It has been shown that fish teeth acquired the Nd isotope composition of bottom seawater during early diagenetic processes that take place at or close to the sediment–water interface (Shaw and Wasserburg, 1985; Martin and

Haley, 2000; Martin and Scher, 2004; Thomas, 2005). Previous studies also suggested that the bottom seawater ε_{Nd} signature recorded by fish teeth is faithfully preserved in sedimentary archives (MacLeod et al., 2008; Martin et al., 2010; Robinson et al., 2010). If this is correct, and although the data are not numerous, the similarity of the $\varepsilon_{Nd(t)}$ of these two archives and the fossil fish teeth signal could suggest that the Fe–Mn oxides coating the foraminifera tests (at Wissant, where both HH-extraction of foraminifera and foraminifera yield a REE profile typical of Fe–Mn oxides) and the calcite of foraminifera (at Hot Spring, where both phases yield a linear REE profile) both record local bottom water $\varepsilon_{Nd(t)}$. The foraminifera recovered from the sediments for Nd isotopic analyses in our study are mixed planktonic foraminifera, both at Hot Spring and at Wissant. This interpretation would imply that the Nd isotopic signal of the planktonic foraminifera calcite, initially acquired in surface waters, has been overprinted by REEs from bottom seawater, or from pore waters having an Nd isotopic composition similar to that of bottom seawater. This would be in agreement with several recent studies showing that the $\varepsilon_{Nd(t)}$ of uncleaned and cleaned planktonic foraminifera at both open sea and margin sites record the Nd isotopic composition of bottom seawater, except for sites displaying easily weathered volcanic ashes (Roberts et al., 2010; Bayon et al., 2011; Elmore et al., 2011).

In contrast, other studies have shown that both uncleaned and cleaned planktonic foraminifera can record the Nd isotopic composition of the surface waters instead of that of bottom waters, possibly through binding of Nd to intratest organic material (Burton and Vance, 2000; Vance et al., 2004; Haley et al., 2005; Martinez-Boti et al., 2009). If the planktonic foraminifera analyzed in this study record a surface water $\varepsilon_{Nd(t)}$, the similarity of foraminifera and HH-extraction of foraminifera Nd isotopic composition with the fish teeth signal would then suggest that both at Wissant and at Hot Spring, the $\varepsilon_{Nd(t)}$ of surface waters was similar to that of the local bottom waters. Both sites are located within a shallow epicontinental sea, with depths of a few hundred meters at most. In a recent study, Carter et al. (2012) has shown that on the Antarctica shelf, boundary exchanges resulted in an Nd isotopic signature of the bottom waters that deviates toward that of the sediments on the first 200 meters of the water column, and that the surface waters had a similar Nd isotopic composition to that of bottom waters. In the large Cretaceous epicontinental seas, boundary exchanges may have been particularly important and have affected the shallow water column on all its extent. Although this remains speculative, it is plausible that the surface water and bottom water could have had a similar $\varepsilon_{Nd(t)}$ signals in these epicontinental seas.

Finally, it has been shown that the Nd isotope composition obtained from Fe–Mn oxides leached from sediments collected on steep continental slopes can be similar to that of seawater at shallower depth (Gutjahr et al., 2008; Stumpf et al., 2010). This can arise when sediments from shallower environments are remobilized and transported downslope. The ε_{Nd} of the Fe–Mn oxides recovered from these sediments, than may include those coating foraminifera and fish teeth in the case of coarser gravity deposits like turbidites, would then reflect a mix between a signal acquired from local bottom waters and a signal acquired from shallower environments. However, as both Hot Spring and Wissant were already located in a quite shallow shelf environment within an epicontinental sea, above the continental slope. It seems therefore unlikely for foraminifera or fish teeth to have been transported from even shallower environments, except through turbitide deposits but these are absent from the two sections.

In one level at Wissant (W12), the $\varepsilon_{Nd(t)}$ of fish teeth is about 2 ε-units higher than that of the Fe–Mn oxide phase of foraminifera. As both HH-extraction of foraminifera and foraminifera gave a similar value, that is in the same range of the levels above and below W12 while the $\varepsilon_{Nd(t)}$ of the fish teeth is significantly higher than that of the fish teeth from the other levels, it is likely that the Nd isotope composition of the fish teeth from W12 may not reflect that of bottom seawater at Wissant. Unfortunately, fish remains were not abundant in this level and it was not possible to replicate the analysis. This may question the reliability of fish teeth as the best phase for recording past seawater ε_{Nd}. Apatite may indeed in some cases continue to incorporate REEs during late diagenesis, as has been suggested by Kocsis et al. (2010). It's possible that the record of the fish tooth from the W12 level as a longer diagenetic history than the contemporaneous Fe–Mn oxides. While Fe–Mn oxides would only form while pore waters are still oxic, fish tooth apatite ε_{Nd} may record a longer diagenetic history. This interpretation is not entirely satisfying though, as it remains difficult to explain why only the fish from one level among those collected would have recorded a longer diagenetic history.

5.2.2. Significance of the $\varepsilon_{Nd(t)}$ of sediments Fe–Mn oxides in the studied shelf environments

In contrast, for the two studied outcrops most of the HH-extraction of sediments exhibit $\varepsilon_{Nd(t)}$ that are intermediate between the detrital fraction and fish teeth (Figs. 5 and 6), although this is not systematic as two samples yielded $\varepsilon_{Nd(t)}$ that are identical to those of fish teeth (W10 and W10bis). This difference toward more negative values for part of the samples suggests a contribution of Fe–Mn oxides pre-formed on continents and brought to the sediments by erosion in these proximal environments. The occurrence of this difference at Hot Springs could be explained if these pre-formed oxides were not all reduced in the possibly anoxic bottom waters that could have prevented authigenic marine oxide formation at the seafloor. Alternatively, leaching of the non-authigenic phases cannot be excluded, resulting in a deviation of the Nd isotope composition of the leachate toward that of the detrital fraction (Roberts et al., 2010; Elmore et al., 2011). Recent Fe–Mn oxides formed after exhumation (telogenesis) of the sediments, in meteoric oxidizing waters, may also have contributed to the signal. In either case, these results suggest that Fe–Mn oxides leached directly from decarbonated sediments cannot be used in proximal, shelf environments to reconstruct the Nd isotope signature of seawater. This interpretation is in accord with previous works on the Nd isotope signature of dispersed Fe–Mn oxides in sediments

at ocean margins (e.g. Bayon et al., 2011; Carter et al., 2012).

5.3. Evolution of shelf seawater ε_{Nd} at the studied sites

5.3.1. Significance of a local shelf seawater Nd isotope signal for paleoceanographic reconstructions

On continental shelves and slopes, where high suspended particle concentrations and dynamic flows tend to remobilize sediments deposited on the margins, favoring exchange of dissolved and particulate Nd, the Nd isotope composition of local bottom seawater can deviate from that of seawater at comparable depth in nearby open ocean settings (Sholkovitz and Szymczak, 2000; Amakawa et al., 2004; Lacan and Jeandel, 2005b; Jeandel et al., 2011; Horikawa et al., 2011; Bayon et al., 2011). A recent study has shown that this deviation toward the Nd isotope composition of the sediments can affect shelf seawater on several hundred meters of the water column above the seafloor (Carter et al., 2012). It is not clear yet whether the $\varepsilon_{Nd(t)}$ of the planktonic foraminifera and of their Fe–Mn oxide coatings reflect the signature of local bottom shelf seawater or of shelf surface seawater. Even in the second case, their similarity with the fish teeth $\varepsilon_{Nd(t)}$ signal implies that these surface waters would then have a Nd isotope signature comparable of that of local bottom waters, whatever the process involved. As a result, we will discuss in the remaining of the paper the significance of the local bottom shelf water $\varepsilon_{Nd(t)}$ at each site. Yet given the shallow depth of the epicontinental seas during the Cretaceous at both sites, we think it likely that a significant part of the water column had been affected by boundary exchanges. As strong diffusive and advective fluxes characterizing the continental margins eventually mix shelf and open ocean seawater (Houghton et al., 1994; Huthnance et al., 2002), the $\varepsilon_{Nd(t)}$ signature of shelf waters contributes to that of nearby open ocean seawawater, independently the origin of the shelf water signal. If changes in surface currents also drive the Nd isotope composition of water masses at oceanic margins, they are more sensitive than open ocean waters to changes in the Nd isotope composition of erosional inputs. Tracking changes in shelf water $\varepsilon_{Nd(t)}$ around an oceanic basin, especially in the areas of deep water sinking, can therefore be useful to interpret the $\varepsilon_{Nd(t)}$ evolution of deep water masses in terms of circulation versus erosional input changes.

5.3.2. Evolution of local shelf seawater Nd isotope signal at the two studied sites

Although speculative, because of the limited the ε_{Nd} data for both sites (7 levels at Wissant and 6 levels at Hot Spring), we present here an attempt to interpret the evolution of the reconstructed local shelf bottom seawater at each studied site.

At Wissant, the inferred $\varepsilon_{Nd(t)}$ signature of bottom shelf seawater during the Albian remains quite unradiogenic, between −8.5 and −9.7 ε-units (Fig. 5A), although still higher by about 1.5–2 ε-units than the detrital fraction. This difference implies that the seawater flowing to each site, prior to any modification by interaction with Nd of detrital origin, should have been more radiogenic than the local sediments. The inferred bottom water values are in agreement with previously published Late Albian fish tooth $\varepsilon_{Nd(t)}$ values from the western Tethys (Pucéat et al., 2005). A westward current along the northern Tethyan margin, that has been inferred based on field evidence (Föllmi and Delamette, 1991), may have brought at this time more radiogenic Pacific waters into the western Tethys. Following this hypothesis, then the more unradiogenic values of about −11 ε-units recorded on the southern Tethyan margin (Soudry et al., 2006) during the Albian would suggest that these more radiogenic water mass inputs likely remained restricted to the northern Tethyan domain. Although the data remain limited, the four levels that have been analyzed for the ε_{Nd} value of the detrital fraction as well show that variations in the reconstructed seawater ε_{Nd} are also mirrored by variations in the same direction of the detrital fraction ε_{Nd} (Fig. 5A). This feature suggests that changes in the Nd signature of local erosional inputs controlled the recorded changes in local bottom seawater $\varepsilon_{Nd(t)}$ in this area, possibly through sediments-seawater interactions (boundary exchange or reversible scavenging).

The Nd isotope values of seawater at Hot Springs are more radiogenic (between −6 and −7 ε-units), and shifted even farther from the values of the detrital fraction, by about 2.5–4 ε-units (Fig. 5B). Ash falls have occurred during the Cenomanian–Turonian interval at Hot Spring, as evidenced by the numerous bentonite levels that have been recognized at this site (Desmares, 2005). None of our samples come from these bentonite levels (levels A–D on Fig. 5B), and the detrital fraction analyzed at this site between the two bentonite levels are quite unradiogenic (−9.4 to −10 ε-units). Yet bentonites represent ash deposits during episodes of exceptionally intense volcanism, and more moderate ash falls, that would not have resulted in the formation of bentonites, are likely to have occurred periodically between the bentonite levels. As volcanic ash is easily weathered, this material may have imprinted the local seawater Nd isotope composition with a more radiogenic value than that of the detrital fraction where possibly remaining ash could have been diluted with clays from eroded nearby continents. In the modern North Pacific, it has been shown that high rates of radiogenic Nd inputs from volcanic islands/arcs can significantly alter the isotopic composition of ambient seawaters (Amakawa et al., 2009; Horikawa et al., 2011).

Alternatively, the large difference between the ε_{Nd} of the inferred bottom seawater and that of the detrital fraction may also reflect an input of quite radiogenic waters at Hot Spring. It has been suggested in the literature that two competing water masses, one from the Arctic, flowing southward, and one from the Proto-Gulf of Mexico, flowing northward, may have influenced the composition of seawater in the Western Interior Seaway (Whittaker and Kyser, 1993; Slingerland et al., 1996; Kump and Slingerland, 1999). To the best of our knowledge, there is no Nd isotope data from the Arctic Ocean available for the mid-Cretaceous, although it has been suggested that this Ocean may have had Pacific-like radiogenic values (typically −5 to

−2 ε-units; Robinson et al., 2010), as it was largely open to the Pacific Ocean (Whittaker and Kyser, 1993). Recent data from Gleason et al. (2009) shows a range of more unradiogenic values for bottom Arctic waters $\varepsilon_{Nd(t)}$ during the Eocene, of −5.5 to −7.5, that are quite comparable to that inferred at Hot Spring in this study. Similarly, there is no Nd data from the Proto-Gulf of Mexico for the Mid-Cretaceous period, although the seawater in this area may have been quite radiogenic as well, as suggested by $\varepsilon_{Nd(t)}$ of around −5 ε-units recorded in the low-latitude western Atlantic (ODP site 1050, Blake Nose; MacLeod et al., 2008).

In contrast to Wissant, the seawater $\varepsilon_{Nd(t)}$ increase of about 1 ε-unit recorded at Hot Springs within the *Neocardioceras juddii* ammonite zone is decoupled from the evolution of the Nd isotope composition of the detrital fraction, that remains more stable and even slightly decreases by about 0.5 ε-unit between the Late Cenomanian and the Early Turonian (Fig. 5B). The inferred shift towards more radiogenic Nd isotopic values for shelf bottom seawater between the levels HS26 and HS28 may reflect an increased amount of more radiogenic waters entering the WIS. Alternatively, this 1 ε-unit increase could be related with an increase of ash falls, either locally or close to the source of the water mass, linked to the massive volcanic eruptions on the Caribbean plateau (Snow et al., 2005). The anomalously high metal abundances recorded in some intervals suggest massive eruptions at the beginning of OAE2 in the WIS that would be synchronous with the increase of the Nd isotope composition of shelf seawater (Snow et al., 2005).

6. CONCLUSION

Although the data presented here need to be completed by additional studies performed in additional depositional contexts, the similarity of the Nd isotope composition of both Fe–Mn coatings of foraminifera and of the carbonate matrix of foraminifera with that of fish teeth in two studied shelf environments provides a route toward the utilization of these archives to reconstruct seawater ε_{Nd} in shallow, proximal environments. In contrast, Fe–Mn oxides leached from decarbonated sediments tend to yield a more negative ε_{Nd} values intermediate between that of fish teeth and of detrital fractions. This suggests that pre-formed continental oxides brought by erosion contribute to the Nd isotope signal in these proximal environments, and that the decarbonated sediment leachate appear less suitable for reconstructions of the Nd isotope signature of shelf seawater.

Although shifted toward more radiogenic values, seawater ε_{Nd} follows a similar evolution during the Late Albian than that of the detrital fraction in the western Tethys. This feature suggests that the evolution of local bottom water ε_{Nd} is controlled by variations in the Nd isotope composition of material eroded from the continent. In contrast, the increase of shelf bottom seawater ε_{Nd} recorded in the Western Interior Seaway during the Late Cenomanian is decoupled from that of the local detrital fraction. This may be related either with an increase of more radiogenic water mass inputs in the studied area, or with a change in the intensity of ash falls, that may have been linked to massive volcanic eruptions on the Caribbean plateau.

ACKNOWLEDGMENTS

We are grateful to E. Ponzevera for support on Nd isotope measurements on the Neptune MC-ICP-MS at the Ifremer, to C. Bassoulet for support on REE analyses, and to F. Magniez-Jannin for her expertise on the foraminifera from the Wissant section. We are indebted to M. Gutjahr and two other anonymous reviewers for their very constructive comments that greatly helped to improve the manuscript. This work was funded by the INSU program SYSTER.

REFERENCES

Amakawa H., Nozaki Y., Alibo D. S., Zhang J., Fukugawa K. and Nagai H. (2004) Neodymium isotopic variations in northwest Pacific waters. *Geochim. Cosmochim. Acta* **68**, 715–727.

Amakawa H., Sasaki K. and Ebihara M. (2009) Nd isotopic composition in the central North Pacific. *Geochim. Cosmochim. Acta* **73**, 4705–4719.

Amédro F. (1992) L'Albien du Bassin Anglo-Parisien: Ammonites, Zonation phylétique, séquences. *Bull. Centre Rech. Explo. Product. Elf Aquit.* **16**(1), 187–233.

Arraes-Mescoff R., Roy-Barman M., Coppola L., Souhaut M., Tachikawa K., Jeandel C., Sempéré R. and Yoro C. (2001) The behavior of Al, Mn, Ba, Sr, REE and Th isotopes during in vitro degradation of large marine particles. *Mar. Chem.* **73**, 1–19.

Arsouze T., Dutay J.-C., Lacan F. and Jeandel C. (2007) Modeling the neodymium isotopic composition with a global ocean circulation model. *Chem. Geol.* **239**, 165–177.

Arsouze T., Dutay J. C., Lacan F. and Jeandel C. (2009) Reconstructing the Nd oceanic cycle using a coupled dynamical–biogeochemical model. *Biogeosciences* **6**(3), 5549–5588.

Arthur M. A., Schlanger S. O. and Jenkyns H. C. (1987) The Cenomanian–Turonian anoxic event, II. Paleoceanographic controls on organic matter production and preservation. In *Marine Petroleum Source Rocks*, vol. 26 (eds. J. Brooks and A. J. Fleet). Geological Society of London, pp. 401–420, Special Publication.

Arthur M. A., Dean W. E. and Pratt L. M. (1988) Geochemical and climatic effects of increased marine organic carbon burial at the Cenomanian/Turonian boundary. *Nature* **335**, 714–717.

Axelsson M. D., Rodushkin I., Ingri J. and Ohlander B. (2002) Multielemental analysis of Mn–Fe nodules by ICP-MS: Optimisation of analytical method. *Analyst* **127**, 76–82.

Asquith D. O. (1970) Depositional topography and major marine environments. *Am. Assoc. Pet. Geol. Bull.* **54**, 1184–1224.

Barrat J. A., Keller F., Amossé J., Taylor R. N., Nesbitt R. W. and Hirata T. (1996) Determination of rare earth element in sixteen silicate reference samples by ICP-MS after T_m addition and ion exchange separation. *Geostand. Newslett.* **20**, 133–139.

Barrat J. A., Zanda B., Moynier F., Bollinger C., Liorzou C. and Bayon G. (2012) Geochemistry of CI chondrites, revisited: Major, trace elements, Cu and Zn isotopes. *Geochim. Cosmochim. Acta* **83**, 79–92.

Basak C., Martin E. E. and Kamenov G. D. (2011) Seawater Pb isotopes extracted from Cenozoïc marine sediments. *Chem. Geol.* **286**, 94–108.

Batt R. (1987) Pelagic biofacies of the Western Interior Greenhorn Sea (Cretaceous): Evidence from ammonites and planktonic foraminifera. Unpublished Ph. D. thesis, Univ. of Colorado. p. 417.

Bayon G., German C. R., Boella R. M., Miltont J. A., Taylor R. N. and Nesbitt R. W. (2002) An improved method for extracting marine sediment fractions and its application to Sr and Nd isotopic analysis. *Chem. Geol.* **187**, 170–199.

Bayon G., German C. R., Burton K. W., Nesbitt R. W. and Rogers N. (2004) Sedimentary Fe–Mn oxyhydroxides as paleoceanographic archives and the role of aeolian flux in regulating oceanic dissolved REE. *Earth Planet. Sci. Lett.* **224**, 477–492.

Bayon G., Barrat J.-A., Etoubleau J., Benoit M., Révillon S. and Bollinger C. (2009) Determination of rare earth elements, Sc, Y, Zr, Ba, Hf and Th in geological samples by ICP-MS after T_m addition and alkaline fusion. *Geostand. Geoanal. Res.* **33**, 51–62.

Bayon G., Birot D., Ruffine L., Caprais J.-C., Ponzevera E., Bollinger C., Donval J.-P., Charlou J.-L. and Voisset M. (2011) Evidence for intense REE scavenging at cold seeps from the Niger Delta margin. *Earth Planet. Sci. Lett.* **312**, 443–452.

Broecker W. S. and Peng T. H. (1982) Tracers in the Sea, report. *Lamont-Doherty Geol. Obs.*, Palisades, N. Y.

Burton K. W. and Vance D. (2000) Glacial-interglacial variations in the neodymium isotope composition of seawater in the Bay of Bengal recorded by planktonic foraminifera. *Earth Planet Sci. Lett.* **176**, 425–441.

Caldwell W. G. E. and Kauffman E. G. (1993) Evolution of the Western Interior Basin. *Geol. Assoc. Can. Spec. Pap.* **39**, 680.

Carter P., Vance D., Hillenbrand C. D., Smith J. A. and Shoosmith D. R. (2012) The neodymium isotopic composition of waters masses in the eastern Pacific sector of the Southern Ocean. *Geochim. Cosmochim. Acta* **79**, 41–59.

De Baar H. J., Bacon M. P., Brewer P. G. and Bruland K. W. (1985) Rare earth elements in the Pacific and Atlantic Oceans. *Geochim. Cosmochim. Acta* **49**, 1943–1959.

Desmares D. (2005) Enregistrement à haute résolution des modifications environnementales inscrites dans un cadre téphrochronologique. Le bassin du Western Interior au passage Cénomanien-Turonien. Ph. D. thesis, Université Louis Pasteur Strasbourg 1, France. p. 440.

Desmares D., Grosheny D., Beaudoin B., Gardin S. and Gauthier-Lafaye F. (2007) High resolution stratigraphic record constrained by volcanic ash beds at the Cenomanian–Turonian boundary in the Western Interior Basin, USA. *Cretac. Res.* **28**, 561–582.

Eicher D. L. and Diner R. (1989) Origin of the Cretaceous Bridge Creek Cycles in the Western Interior, United States. *Palaeogeogr. Palaeoclimatol. Palaeoecol.* **74**, 127–146.

Elder, W. P. 1987. Cenomanian–Turonian (Cretaceous) stage boundary extinctions in the Western Interior of the United States. Ph. D. thesis, Univ. of Colorado. p. 621.

Elderfield H., Hawkesworth C. J., Greaves M. J. and Calvert S. E. (1981) Rare earth element zonation in Pacific ferromanganese nodules. *Geochim. Cosmochim. Acta* **45**, 1231–1234.

Elderfield H., Upstill-Goddard R. and Sholkovitz E. R. (1990) The rare earth elements in rivers, estuaries, and coastal seas and their significance to the composition of ocean waters. *Geochim. Cosmochim. Acta* **54**, 971–991.

Elderfield H. and Pagett R. (1986) REE in ichthyoliths; variations with redox conditions and depositional environment. *Sci. Total Env.* **49**, 175–197 (Spec Issue in Honour of J.P. Riley).

Elderfield H. and Sholkovitz E. R. (1987) Rare earth elements in the pore waters of reducing nearshore sediments. *Earth Planet. Sci. Lett.* **82**, 280–288.

Elmore A. C., Piotrowski A. M., Wright J. D. and Scrivner A. E. (2011) Testing the extraction of past seawater Nd isotopic composition from North Atlantic deep sea sediments and foraminifera. *Geochem. Geophys. Geosys.* **12**, Q09008. http://dx.doi.org/10.1029/2011GC003741.

Föllmi K. B. and Delamette M. (1991) Model simulation of Mid-Cretaceous ocean circulation: Technical comments. *Science* **251**, 94–95.

Frank M. (2002) Radiogenic isotopes: Tracers of past ocean circulation and erosional input. *Rev. Geophys.* **40**(1), 1–38.

Friedrich O., Erbacher J., Moriya K., Wilson P. A. and Kuhnert H. (2008) Warm saline intermediate waters in the Cretaceous tropical Atlantic Ocean. *Nat. Geosci.* **1**, 453–457.

German C. R. and Elderfield H. (1990) Application of the Ce anomaly as a paleoredox indicator: The ground rules. *Paleoceanography* **5**(5), 823–833.

Gleason J. D., Thomas D. J., Moore, Jr., T. C., Blum J. D., Owen R. M. and Haley B. A. (2009) Early to middle Eocene history of the Arctic Ocean from Nd–Sr isotopes in fossil fish debris Lomonosov Ridge. *Paleoceanography* **24**, PA2215. http://dx.doi.org/10.1029/2008PA001685.

Goldstein S. L. and O'Nions R. K. (1981) Nd and Sr isotopic relationships in pelagic clays and ferromanganese deposits. *Nature* **292**, 324–327.

Gourlan A. T. (2006) Stratigraphie isotopique du néodyme dans l'océan Indien: Paléocirculation océanique et érosion continentale. Ph. D. thesis. Université Paris VII Denis Diderot. p. 180.

Gourlan A. T., Meynadier L., Allègre C. J., Tapponnier P., Birck J. L. and Joron J. L. (2010) Northern Hemisphere climate control of the Bengali rivers discharge during the past 4 Ma. *Quatern. Sci. Rev.* **29**, 2484–2498.

Gradstein F., Ogg J. and Smith A. (2004) *A Geologic Time Scale 2004*. Cambridge University Press, Cambridge.

Grandjean P., Cappetta H., Michard A. and Albarède F. (1987) The assessment of REE patterns and $^{143}Nd/^{144}Nd$ ratios in fish remains. *Earth Planet. Sci. Lett.* **84**, 181–196.

Gutjahr M., Frank M., Stirling C. H., Klemm V., Van de Flierdt T. and Halliday A. N. (2007) Reliable extraction of a deepwater trace metal isotope signal from Fe–Mn oxyhydroxide coatings of marine sediments. *Chem. Geol.* **242**, 351–370.

Gutjahr M., Frank M., Stirling C. H., Keigwin L. D. and Halliday A. N. (2008) Tracing the Nd isotope evolution of North Atlantic deep and intermediate waters in the western North Atlantic since the Last Glacial Maximum from Blake Ridge sediments. *Earth Planet. Sci. Lett.* **266**, 61–77.

Gutjahr M., Hoogakker B. A. A., Frank M. and McCave I. N. (2010) Changes in north Atlantic deep water strength and bottom water masses during marine isotope stage 3 (45–35 ka BP). *Quatern. Sci. Rev.* **29**, 2451–2461.

Haley B. A., Klinkhammer G. P. and Mc Manus J. (2004) Rare earth elements in pore waters of marine sediments. *Geochim. Cosmochim. Acta* **68**, 1265–1279.

Haley B. A., Klinkhammer G. P. and Mix A. C. (2005) Revisiting the rare earth elements in foraminiferal tests. *Earth Planet. Sci. Lett.* **239**, 79–97.

Hay W. W., Eicher D. L. and Diner R. (1993) Physical oceanography and water masses in the Cretaceous Western Interior seaway. In *Evolution of the Western Interior Basin* (eds. W. G. E. Caldwell and E. G. Kauffman), pp. 297–318. vol. 39. Geological Association of Canada, Special Paper.

Hay W. W. (2008) Evolving ideas about the Cretaceous climate and ocean circulation. *Cretac. Res.* **29**, 725–753.

Houghton R. W., Flagg C. N. and Pietrafesa L. J. (1994) Shelf-slope water frontal structure, motion and eddy heat-flux in the southern Middle Atlantic Bight. *Deep-Sea Res. II* **41**, 273–306.

Horikawa K., Martin E. E., Asahara Y. and Sagouva T. (2011) Limits on conservate behavior of Nd isotopes in seawater assessed from analysis of fish teeth from Pacific core tops. *Earth Planet. Sci. Lett.* **310**, 119–130.

Huthnance J. M., Van Aken H. M., White M., Barton E. D., Le Cann B., Coelho E. F., Fanjul E. A., Miller P. and Vitorino J.

() Ocean margin exchange-water flux estimates. *J. Mar. Syst.* **32**, 107–137.

Jacobsen S. B. and Wasserburg G. J. (1980) Sm–Nd isotopic evolution of chondrites. *Earth Planet. Sci. Lett.* **50**, 139–155.

Jeandel C., Arsouze T., Lacan F., Téchiné P. and Dutay J.-C. (2007) Isotopic Nd compositions and concentrations of the lithogenic inputs into the ocean: A compilation, with an emphasis on the margins. *Chem. Geol.* **239**, 156–164.

Jeandel C., Peucker-Ehrenbrink B., Jones M. T., Pearce C. R., Oelhers E. H., Godderis Y., Laccan F., Aumont O. and Arsouze T. (2011) Ocean margins: The missing term in oceanic element budgets? *Eos* **92**, 217–224.

Johannesson K. H. and Burdige D. J. (2007) Balancing the global oceanic neodymium budget: Evaluating the role of groundwater. *Earth Plant. Sci. Lett.* **253**, 129–142.

Jordan T. E. (1991) Thrust loads and foreland basin evolution, Cretaceous, western United States. *Am. Assoc. Pet. Geol. Bull.* **65**, 2506–2520.

Kauffman E. G. (1977) Geological and biological overview: Western Interior Cretaceous Basin. *Mountain Geol.* **14**, 75–99.

Khan M. H. (1950) Note on the depth and temperature of the Gault Sea as indicated by Foraminifera. *Geol. Mag.* **87**, 175–180.

Klevenz V., Vance D., Schmidt D. N. and Mezger K. (2008) Neodymium isotopes in benthic foraminifera: Core-top systematic and a down-core record from the Neogene south Atlantic. *Earth Planet. Sci. Lett.* **265**, 571–587.

Knight R. I. (1997) Benthic palaeoecology of the Gault Clay Formation (Mid-and basal Upper Albian) of the western Anglo-Paris Basin. *Proc. Geol. Assoc.* **108**, 81–103.

Kocsis L., Trueman C. N. and Palmer M. R. (2010) Protracted diagenetic alteration of REE contents in fossil bioapatites: Direct evidence from Lu–Hf isotope systematic. *Geochim. Cosmochim. Acta* **74**, 6077–6092.

Koppenkastrop D. and De Carlo (1992) Sorption of rare earth elements from seawater onto synthetic mineral particles: An experimental approach. *Chem. Geol.* **95**, 251–263.

Kump L. R. and Slingerland R. L. (1999) Circulation and stratification of the early Turonian Western Interior Seaway: Sensitivity to a variety of forcings. In *Evolution of the Cretaceous Ocean-Climate*, vol. 332 (eds. E. Barrera and C. C. Johnson). Geological Society of America, pp. 181–190, Special paper.

Lacan F. and Jeandel C. (2004a) Denmark Strait water circulation traced by heterogeneity in neodymium isotope compositions. *Deep-Sea Res.* **51**, 71–82.

Lacan F. and Jeandel C. (2004b) Neodymium isotopic composition and rare earth element concentrations in the deep and intermediate Nordic Seas: Constraints on the Iceland Scotland Overflow Water signature. *Geochem. Geophys. Geosys.* **5**, Q11006. http://dx.doi.org/10.1029/2004GC000742.

Lacan F. and Jeandel C. (2004c) Subpolar Mode Water formation traced by neodymium isotopic composition. *Geophys. Res. Lett.* **31**, L14306. http://dx.doi.org/10.1029/2004GL019747.

Lacan F. and Jeandel C. (2005a) Neodymium isotopes as a new tool for quantifying exchange fluxes at the continent–ocean interface. *Earth Planet. Sci. Lett.* **232**, 245–257.

Lacan F. and Jeandel C. (2005b) Acquisition of the neodymium isotopic composition of the North Atlantic Deep Water. *Geochem. Geophys. Geosys.* **6**, Q12008. http://dx.doi.org/10.1029/2005GC00956.

Leckie R. M., Yuretich R. F., West O. L. O., Finkelstein D. and Schmidt M. (1998) Paleoceanography of the southwestern Western Interior Sea during the time of the Cenomanian–Turonian boundary (Late Cretaceous). *Soc. Sediment. Geol.* **6**, 101–126.

Lugmair G. W. and Marti K. (1977) Sm–Nd-Pu timepieces in the Angra dos Reis meteorite. *Earth Planet. Sci. Lett.* **35**, 273–284.

Macleod K. G., Martin E. E. and Blair S. W. (2008) Nd isotopic excursion across Cretaceous Ocean Anoxic Event 2 (Cenomanian/Turonian) in the tropical North Atlantic. GSA. *Geology* **36**(10), 811–814.

Martin E. E. and Haley B. A. (2000) Fossil fish teeth as proxies for seawater Sr and Nd isotopes. *Geochim. Cosmochim. Acta* **64**(5), 835–847.

Martin E. E. and Scher H. D. (2004) Preservation of seawater Sr and Nd isotopes in fossil fish teeth: Bad news and good news. *Earth Planet. Sci. Lett.* **220**, 25–39.

Martin E. E., Blair S. W., Kamenov G. D., Scher H. D., Bourbon E., Bask C. and Newkirk D. N. (2010) Extraction of Nd isotopes from bulk deep sea sediments for paleoceanographic studies on Cenozoic time scales. *Chem. Geol.* **269**, 414–431.

Martin E. E., MacLeod K. G., Jiménez-Berrocoso A. and Bourbon E. (2012) Water mass circulation on Demerara Rise during the Late Cretaceous based on Nd isotopes. *Earth Planet. Sci. Lett.* **328**, 111–120.

Martinez-Boti M. A., Vance D. and Mortyn P. G. (2009) Nd/Ca ratios in plankton-towed and core top foraminifera: Confirmation of the water column acquisition of Nd. *Geochem. Geophys. Geosys.* **10**, Q08018, 101029/2009GC002701.

Négrel P., Casanova J. and Brulhet J. (2006) REE and Nd isotope stratigraphy of a Late Jurassic carbonate platform, eastern Paris Basin, France. *J. Sediment. Res.* **76**, 605–617.

Palmer M. R. (1985) Rare earth elements in foraminifera tests. *Earth Planet. Sci. Lett.* **73**, 285–298.

Palmer M. R. and Elderfield H. (1985) Variations in the Nd isotopic composition of foraminifera from Atlantic Ocean sediments. *Earth Planet. Sci. Lett.* **73**, 299–305.

Picard S., Lécuyer C., Barrat J. A., Garcia J. P., Dromart G. and Sheppard S. M. F. (2002) Rare earth element contents of Jurassic fish and reptile teeth and their potential relation to seawater composition (Anglo-Paris Basin, France and England). *Chem. Geol.* **186**, 1–16.

Piepgras D. J., Wasserburg G. J. and Dasch E. J. (1979) The isotopic composition of Nd in different ocean masses. *Earth Planet. Sci. Lett.* **45**, 233–236.

Piepgras D. J. and Wasserburg G. J. (1987) Rare earth transport in the western North Atlantic inferred from isotopic observations. *Geochim. Cosmochim. Acta* **51**(1257), 1271.

Piepgras D. J. and Jacobsen S. B. (1988) The isotopic composition of neodymium in the North Pacific. *Geochim. Cosmochim. Acta* **52**, 1373–1381.

Piepgras D. J. and Jacobsen S. B. (1992) The behavior of rare-earth elements in seawater precise determination of variations in the North Pacific water column. *Geochim. Cosmochim. Acta* **56**, 1851–1862.

Pin C. and Zalduegui J. F. S. (1997) Sequential separation of light rare-earth elements, thorium and uranium by miniaturized extraction chromatography: Application to isotopic analyses of silicate rocks. *Anal. Chim. Acta* **339**, 79–89.

Piotrowski A. M., Goldstein S. L., Hemming S. R. and Fairbanks R. G. (2004) Intensification and variability of ocean thermohaline circulation through the last deglaciation. *Earth Planet. Sci. Lett.* **225**, 205–220.

Piotrowski A. M., Goldstein S. V., Hemming S. R. and Fairbanks R. G. (2005) Temporal relationships of carbon cycling and ocean circulation at glacial boundaries. *Science* **307**, 1933–1938.

Piotrowski A. M., Goldstein S. L., Hemming S. R., Fairbanks R. G. and Zylberberg D. R. (2008) Oscillating glacial northern and southern deep water formation from combined neodymium and carbon isotopes. *Earth Planet. Sci. Lett.* **272**, 394–405.

Pucéat E., Lécuyer C. and Reisberg L. (2005) Neodymium isotope evolution of NW Tethyan upper ocean waters throughout the Cretaceous. *Earth Planet. Sci. Lett.* **236**, 705–720.

Rempfer J., Stocker T. F., Joos F., Dutay J. C. and Siddall M. (2011) Modelling Nd-isotopes with a coarse resolution ocean circulation model: Sensitivities to model parameters and source/sink distributions. *Geochim. Cosmochim. Acta* **75**, 5927–5950.

Reynard B., Lécuyer C. and Grandjean P. (1999) Crystal-chemical controls on rare-earth element concentrations in fossil biogenic apatites and implications for paleoenvironmental reconstructions. *Chem. Geol.* **155**, 233–241.

Robaszynski F., Amédro F., Foucher J. C., Gaspard D., Magniez-Jannin F., Manivit H. and Sornay J. (1980) Synthèse biostratigraphique de l'Aptien au Santonien du Boulonnais à partir de sept groupes paléontologiques: Foraminifères, Nannoplancton, Dinoflagellés et Macrofaunes. In Rev. Micropaleont., vol. 22, pp. 195–321.

Robaszynski F. and Amédro F. (1993) Les falaises Crétacé du Boulonnais. La coupe de référence du Cap Blanc Nez dans le contexte sédimentaire global. *Ann. Soc. Geol. Nord.* **2**(2), 31–44.

Roberts N. L., Piotrowski A. M., McManus J. F. and Keigwin L. D. (2010) Synchronous deglacial overturning and water mass source changes. *Science* **327**, 75–78.

Robinson S. A., Murphy D. P., Vance D. and Thomas D. J. (2010) Formation of Southern component Water in the Late Cretaceous: Evidence from Nd-isotopes. *Geology* **38**(10), 871–874.

Rongemaille E., Bayon G., Pierre C., Bollinger C., Chu N. C., Favreau E., Fouquet Y., Riboulot V. and Voisset M. (2011) Rare earth elements in cold seep carbonates from the Niger Delta. *Chem. Geol.* **286**, 196–206.

Rutberg R. L., Hemming S. R. and Goldstein S. L. (2000) Reduced North Atlantic Deep Water flux to the glacial Southern Ocean inferred from neodymium isotope ratios. *Nature* **405**, 935–938.

Sageman B. B. and Arthur M. A. (1994) Early Turonian paleogeographic/paleobathymetric map, Western Interior, U.S. In *Mesozoic Systems of the Rocky Mountain Region, USA* (eds. M. V. Caputo, J. A. Peterson and K. J. Franczyk). SEPM, Rocky Mountain Section. pp. 457–470.

Sageman B. B., Meyers S. R. and Arthur M. A. (2006) Orbital time scale and new C-isotope record for Cenomanian–Turonian boundary stratotype. *Geol. Soc. Am.* **34**, 125–128.

Schields G. A. and Webb G. E. (2004) Has the REE composition of seawater changed over geological time? *Chem. Geol.* **204**, 103–107.

Shimizu H., Tachikawa K., Masuda A. and Nozaki Y. (1994) Cerium and neodymium ratios and REE patterns in seawater from the North Pacifc Ocean. *Geochim. Cosmochim. Acta* **58**, 323–333.

Shaw H. F. and Wasserburg G. J. (1985) Sm, Nd in marine carbonates and phosphates. *Geochim. Cosmochim. Acta* **49**, 503–518.

Sholkovitz E. and Szymczak R. (2000) The estuarine chemistry of rare earth elements: Comparison of the Amazon, Fly, Sepik and the Gulf of Papua systems. *Earth Planet. Sci. Lett.* **179**, 299–309.

Slingerland R. L., Kump L. R., Arthur M. A., Sageman B. B. and Barron E. J. (1996) Estuarine circulation in the Turonian Western Interior Seaway of North America. *Geol. Soc. Am. Bull.* **108**, 941–952.

Siddall M., Khatiwala S., van de Flierdt T., Jones K., Goldstein S. L., Hemming S. and Anderson R. (2008) Towards explaining the Nd paradox using reversible scavenging in an ocean general circulation model. *Earth Planet. Sci. Lett.* **274**, 448–461.

Snow L. J., Duncan R. A. and Bralower T. J. (2005) Trace element abundances in the Rock Cayon Anticline, Pueblo, Colorado, marine sedimentary section and their relationship to Carribean plateau construction and oxygen anoxic event 2. *Palaeoceanography* **20**, 1–14.

Soudry D., Glenn C. R., Nathan Y., Segal I. and Vonderhaar D. (2006) Evolution of Tethyan phosphogenesis along the northern edges of the Arabian–African shield during the Cretaceous–Eocene as deduced from temporal variations of Ca and Nd isotopes and rates of P accumulation. *Earth-Sci. Rev.* **78**, 27–57.

Stumpf R., Frank M., Schönfeld J. and Haley B. A. (2010) Late Quaternary variability of Mediterranean outflow water from radiogenic Nd and Pb isotopes. *Quatern. Sci. Rev.* **29**, 2462–2472.

Tachikawa K., Athias V. and Jeandel C. (2003) Neodymium budget in the modern ocean and paleo-oceanographic implications. *J. Geophys. Res. Oceans* **108**, 32–54.

Taylor S. R. and McLennan S. M. (1985) *The Continental Crust: Its Composition and Evolution*. Blackwell, Oxford, p. 312.

Thomas D. J. (2004) Evidence for deep-water production in the North Pacific Ocean during the early Cenozoic warm interval. *Nature* **430**, 65–68.

Thomas D. J. (2005) Reconstructing ancient deep-sea circulation patterns using the Nd isotopic composition of fossil fish debris. In *Isotopic and Elemental Tracers of Late Cenozoic Climate Change*, vol. 395, pp. 1–12. Isotopic and Elemental Tracers of Late Cenozoic Climate Change. GSA Spec. Pub..

Vance D. and Burton K. (1999) Neodymium isotopes in planktonic foraminifera: A record of the response of continental weathering and ocean circulation rates to climate change. *Earth Planet. Sci. Lett.* **173**, 365–379.

Vance D., Scrivner A. E., Beney P., Staubwasser M., Henderson G. M. and Slowey N. C. (2004) The use of foraminifera as a record of the past neodymium isotope composition of seawater. *Paleoceanography* **19**, PA2009. http://dx.doi.org/10.1029/2003PA000957.

Vrielynck B. and Bouysse P. (2003) Le visage changeant de la Terre. *Comission de la carte géologique du monde*. Editions UNESCO (Paris, France).

Weimer R. J. (1984) Relationship of unconformities, tectonics, and sea level changes in the cretaceous of the western interior, United States. In *Interregional Unconformities and Hydrocarbon Accumulation*, vol. 36 (ed. J. S. Schlee). AAPG Memoir, pp. 7–35.

Whittaker S. G. and Kyser T. K. (1993) Variations in the neodymium and strontium isotopic composition and REE content molluscan shells from the Cretaceous Western Interior seaway. *Geochim. Cosmochim. Acta* **57**, 4003–4014.

Zhang Y., Lacan F. and Jeandel C. (2008) Dissolved rare earth elements tracing lithogenic inputs over the Kerguelen Plateau (Southern Ocean). *Deep-Sea Res., Part 2. Top. Stud. Oceanogr.* **55**, 638–652.

Ziegler P. A. (1990) Collision related intra-plate compression deformations in Western and Central Europe. *J. Geodyn.* **11**, 357–388.

Associate editor: Mark Rehkamper